1-1-2013

Computational Representation of the Patellofemoral Joint

Abraham Wright
University of Denver

Computational Representation of the Patellofemoral Joint

Abstract

Many people suffer from knee pain due to abnormal function of the patellofemoral joint and are not able to enjoy normal activities of daily living. Surgical treatments are available and new methods are being developed by the medical industry. However, computational tools to efficiently evaluate the effects of the intervention on patellofemoral function are lacking.

Therefore, a validated and efficient computational model of the patellofemoral joint was developed. The subject specific finite element model was validated against the patellar kinematics recorded during cadaveric patellofemoral laxity experiments of the natural knee. The development involved a sequential process in which the soft-tissue was represented with an increasingly more mechanistic approach with each model iteration. Medial and lateral PF laxity models were developed with the knee at several flexion angles (full extension, ~25 degrees, and ~60 degrees), and a model to simulate passive range of motion was also created.

Optimization was conducted to fine-tune a selection of soft-tissue parameters in order to minimize the difference between model-predicted and experimental kinematic results. The average RMS differences for all degrees of freedom and for all flexion angles tested were 2.4 mm and 6.7 degrees with the most simplistic model iteration and 2.5 mm and 5.2 degrees with the most complex model iteration. When the RMS results for medial and lateral PF laxity models are isolated, an improvement is noticed for the most complex iteration's medial laxity results with average RMS differences of 1.6 mm and 4.4 degrees. The validated PF laxity model can be used to assess how changes in knee geometry affect factors such as soft tissue tension and patella tracking.

Document Type

Thesis

Degree Name

M.S.

Department

Mechanical Engineering

First Advisor

Paul J. Rullkoetter

Second Advisor

Peter Laz

Third Advisor

Chris Hughen

Keywords

Computational, Finite element, Knee, Patellofemoral

Subject Categories

Biomedical Devices and Instrumentation | Biomedical Engineering and Bioengineering | Engineering

COMPUTATIONAL REPRESENTATION OF THE PATELLOFEMORAL JOINT

_____

A Thesis

Presented to

The Faculty of Engineering and Computer Science

University of Denver

_____

In Partial Fulfillment

of the Requirements for the Degree

Master of Science

_____

by

Abraham P. Wright

March 2013

Advisor: Paul J. Rullkoetter

Author: Abraham P. Wright
Title: COMPUTATIONAL REPRESENTATION OF THE PATELLOFEMORAL JOINT
Advisor: Paul J. Rullkoetter
Degree Date: March 2013

Abstract

Many people suffer from knee pain due to abnormal function of the patellofemoral joint and are not able to enjoy normal activities of daily living. Surgical treatments are available and new methods are being developed by the medical industry. However, computational tools to efficiently evaluate the effects of the intervention on patellofemoral function are lacking.

Therefore, a validated and efficient computational model of the patellofemoral joint was developed. The subject specific finite element model was validated against the patellar kinematics recorded during cadaveric patellofemoral laxity experiments of the natural knee. The development involved a sequential process in which the soft-tissue was represented with an increasingly more mechanistic approach with each model iteration. Medial and lateral PF laxity models were developed with the knee at several flexion angles (full extension, ~25 degrees, and ~60 degrees), and a model to simulate passive range of motion was also created.

Optimization was conducted to fine-tune a selection of soft-tissue parameters in order to minimize the difference between model-predicted and experimental kinematic results. The average RMS differences for all degrees of freedom and for all flexion angles tested were 2.4 mm and 6.7 degrees with the most simplistic model iteration and 2.5 mm and 5.2 degrees with the most complex model iteration. When the RMS results for medial and lateral PF laxity models are isolated, an improvement is noticed for the

most complex iteration's medial laxity results with average RMS differences of 1.6 mm and 4.4 degrees. The validated PF laxity model can be used to assess how changes in knee geometry affect factors such as soft tissue tension and patella tracking.

Acknowledgements

First and foremost, I would like to thank my wife, Lisa, for her constant support and encouragement over the past few years while finishing my degree and at the same time starting a new family with two wonderful children. I would also like to thank my advisor, Professor Paul Rullkoetter, for suggesting that I continue my education and his guidance. Many others at University of Denver and DePuy helped me along the way, including James Deacey, Clare Fitzpatrick, Chandru Rao, Professor Pete Laz, and Chadd Clary. It was tremendously rewarding to collaborate with them and their assistance was critical to the success of this research. Finally, I would like to thank DePuy Orthopaedics for their commitment to developing employees and advancing the science of knee replacement.

Table of Contents

List of Tables

List of Figures

CHAPTER ONE: INTRODUCTION

Healthy function of the knee joint is critical for enjoying a mobile lifestyle in which activities such as walking, squatting, and kneeling are expected. However, many people suffer from knee pain resulting from abnormal function of the patella and surrounding soft-tissues. Specifically, some patients suffer from patella dislocation where the patella does not engage appropriately with the mating geometry of the femur. Also, it is common for patients who have undergone total knee replacement to experience anterior knee pain, which leads to decreased mobility and patient satisfaction. Several causes of anterior knee following total knee replacement have been hypothesized, including improper patella tracking and excessive strain in the soft-tissues that surround the patella.

A proper understanding of the function of the patella is critical in determining appropriate interventions for patients suffering from anterior knee pain. It is equally important to know what secondary consequences the surgical intervention might have on patellar function. Cadaveric evaluations are important tools in being able to evaluate surgical treatments. However, they require large amount of resources in terms of both time and money, and therefore limit the number of evaluations that may be performed. Computational models on the other hand provide an efficient method of evaluating many treatment variations with minimal resource expense. Therefore, it was the goal of the present study to develop a validated and computationally efficient model of the

patellofemoral joint that could be subsequently used to investigate the effects of surgical interventions on the function of the patella and surrounding soft-tissues.

Anatomy of the Patellofemoral Joint

The patellofemoral (PF) joint is considered the third compartment of the largest joint in the human body, the knee. The PF joint consists of the patella, the distal end of the femur, and the surrounding soft-tissues. As the knee bends, increasingly larger forces are required to maintain higher degrees of flexion (Sharma et al. 2008). Therefore, a principal role of the patella is to provide mechanical advantage to the lower limb extensor mechanism by articulating with the distal end of the femur. In terms of kinematics, the majority of the motion of the patella is in the sagittal plane. However, the patella also experiences out-of-plane movement relative to the femur. The out-of-plane motion and subsequent medial-lateral stability of the PF joint are influenced by a complex interaction between the articular surfaces of the patella and femur, the muscle forces, and the passive soft-tissue restraints (Amis et al. 2003).

The articular stabilizers of the PF joint consist of the cartilaginous surfaces of the patella bone and the femoral trochlear groove. In normal healthy knees, the trochlear groove is formed between medial and lateral convex surfaces (Figure 1.1) that guide the patella from a proximal position on the femur in early flexion to a more distal position between the medial and lateral condyles in deep flexion (Shih et al. 2004; Tecklenburg et al. 2006). Various studies have investigated the orientation of the trochlear groove and reported conflicting results (Barink et al. 2003; Iranpour et al. 2010; Shih et al. 2004),

which are likely caused by differences in landmarks chosen to create reference systems (Iranpour et al.). The articular surface of the patella is shaped into three medial and three lateral facets that articulate with the trochlear groove during knee flexion, and a seventh facet on the medial side that articulates only in deep flexion (Figure 1.2) (Tecklenburg et al.). The patella has a median ridge that is offset medially by approximately three millimeters, allowing the patella to maintain a lateral position throughout the range of motion (Baldwin and House 2005; Yoo et al. 2007).

The six muscles that form the quadriceps mechanism also provide stability to the PF joint (Figure 1.3). The vastus intermedius (VI) is situated in the quadriceps' deep layer and attaches to the proximal pole of the patella (Terry 1989). The rectus femoris (RF), vastus lateralis 1ongus (VLL), and vastus medialis 1ongus (VML) comprise the intermediate layer (Terry). This layer also attaches proximally to the patella, but continues over the anterior surface of the patella and transitions into the patella tendon on the distal pole of the patella (Terry). The patella tendon then continues distally until it attaches to the tibial tubercle. The superficial layer consists of the vastus lateralis ob1iquus (VLO) and vastus medialis ob1iquus (VMO), which integrate with the retinaculum and attach to the lateral and medial margins of the patella, respectively (Farahmand et al.). Cross-sectional analysis of cadaveric specimens has shown that the VI and RF, which are approximately parallel to the long-axis of the femur, contribute 35% of the muscle force on average (Farahmand et al.). The VLL and VMO contribute 34% and 10%, respectively, and the VML and VMO contribute a lesser amount of 15% and 10%, respectively (Farahmand et al.).

The final contribution to PF stability comes from a number of passive soft-tissue restraints that attach the patella to surrounding structures. The restraints are thin ligaments that form a complex fibrous network on both the medial and lateral sides of the knee to make up the medial and lateral retinacula. Despite the complexity of the retinacula, distinct ligaments can be observed on both the medial and lateral sides during dissection and evaluated in terms of their influence on patella stability. On the medial side, three important structures are the medial patellofemoral ligament (MPFL), medial patellotibial ligament (MPTL), and the medial patellomeniscal ligament (MPML).

The MPFL, which connects the superomedial aspect of the patella to the medial side of the femur, has been well defined anatomically in the literature due to interest in appropriate MPFL reconstruction for patients with recurrent patella subluxation. The MPFL is located in the second fascial layer of the knee, superficial to the joint capsule, and passes underneath the vastus medialis to insert into the medial margin of the patella (Warren et al. 1979; Dirim et al. 2008; Baldwin J.L., 2009). The width of the MPFL decreases as it spans from the patella to the femur, ranging in width from approximately 17 to 32 mm at the patellar insertion and 8 to 16 mm at the femoral attachment (Philippot et al. 2009). The femoral MPFL attachment has been reported in two studies (Conlan, et al. 1993; Tuxoe et al. 2002) as originating at the adductor tubercle. More recent studies, however, have identified the MPFL femoral attachment as being located between the medial epicondyle and adductor tubercle, rather than just on the adductor tubercle and the studies have quantified the location relative to the bony landmarks. Nomura et al. (2005) found the center of the anterior border of the MPFL's femoral attachment to be 9.5 ± 1.8 mm proximal and 5.0 ± 1.7 mm posterior to the medial femoral epicondyle. LaPrade et

al. (2007) reported that the center of the MPFL femoral attachment on average was located 10.6 mm (range, 8.0 to 13.4 mm) proximally and 8.8 mm (range, 6.7 to 10.3 mm) posteriorly to the medial epicondyle. Philippot, et al. (2009) also found the center of MPFL femoral attachment to be approximately 10 mm posterior to the epicondyle and 10 mm distal to the adductor tubercle. The location of the MPFL's femoral attachment allows the ligament to tighten in full extension and slacken as the knee flexes (Stephen et al. 2012).

The patella is connected distally to the tibia via the MPTL and MPML. Both ligaments are located in the third fascial layer of the medial retinaculum and are thinner than the MPFL (Thawait et al. 2012). The MPTL inserts into the inferior and medial margin of the patella and the proximal portion of the patella tendon (Dirim et al. 2008, Thawait et al. 2012). The ligament spans from the patella to the medial side of the tibia where it attaches inferior to the joint line (Dirim et al. 2008). The MPML extends from the inferior and medial aspect of the patella and attaches to the anterior rim of the medial meniscus (Dirim et al. 2008, Thawait et al. 2012).

The lateral side of the knee also has a multi-layered retinaculum consisting of thin ligaments that provide passive restraint to the patella. However, the ligaments are less distinct from the overall retinacular geometry than on the medial side and are more appropriately labeled as condensations of the lateral joint capsule rather than individual ligaments (Merican et al. 2007). Therefore, due to the complex geometry, the lateral layers and structures are inconsistently and less defined in the literature (Merican et al. 2007, Thawait et al. 2012). However, four distinct structures have been proposed in the literature: the lateral patellofemoral ligament (LPFL), lateral patellomeniscal ligament

(LPML), lateral patellotibial ligament (LPTL), and the iliotibial band-patella fibers (Merican et al. 2007, Thawait et al. 2012). Similar to the medial side of the knee, the lateral patellofemoral, patellomeniscal, and patellotibial ligaments attach the patella to the femur, meniscus, and tibia, respectively. In contrast to the medial side, the LPFL has been reported to attach directly to the lateral epicondyle and the LPTL to attach to the tibia between the tibial and Gerdy's tubercles (Merican et al. 2007). Also, the lateral side of the knee has a band of relatively thick transverse fibers that attach the lateral margin of the patella to the iliotibial band, and which has been termed the iliotibial band-patella fibers by Merican et al. (2007). The iliotibial band-patella fibers only attach to the iliotibial band and do not provide attachment directly to bone.

Structural Properties of Patellar Ligaments

As mentioned above, peri-patellar ligaments attach the patella bone to surrounding structures, thereby providing stability to the patella as it moves during knee flexion. Structural properties for a selection of the peri-patella ligaments are found in the literature. Staubli et al. (1999) tested the mechanical tensile properties of preconditioned quadriceps and patella tendons that were cut down to a uniform width of 10 mm. The ultimate stresses for the quadriceps and patella tendons were 38.0 ± 5.0 Pa and 69.6 ± 8.3 Pa, respectively. The average ultimate strains for the quadriceps and patella tendons were 11.2 ± 2.2 % and 14.4 ± 3.3 %, respectively. Significant differences were noted between the quadriceps and patella tendons in both stress and strain properties. Mountney et al. (2005) reported the tensile strength of the MPFL to be 208 ± 90 N with

elongation of 26 ± 7 mm. Merican et al. (2009) tested the tensile properties for three structures of the lateral retinaculum: the iliotibial band-patella band (i.e. iliotibial band-patella fibers), the LPFL, and the LPML. The results demonstrated that the iliotibial band-patella fibers were significantly stronger than the other two lateral ligaments with a tensile strength of 582 ± 193 N. The LPFL exhibited a maximum tensile strength of 172 ± 55 N and elongation of 23 ± 6 mm, which were similar results to the strength and elongation properties reported by Mountney et al. for the MPFL. The LPML tensile strength was 85 ± 52 N with elongation of 14 ± 4 mm.

Patellofemoral Stability

The literature contains various articles on the role of anatomy in contributing to PF stability. In terms of soft tissue restraint, numerous selective cutting studies have been conducted to isolate the contributions provided by the MPFL, medial retinaculum, MPML, and MPTL. Conlan et al. (1993) and Desio et al. (1998) conducted similar studies in which cadaveric knees were tested in full extension and at 20 degrees of knee flexion, respectively. Both studies found that the MPFL provided the most restraint to lateral motion with 53% to 60% of the total force on average. The studies also ranked the remaining structures in the same order with the MPML providing the second most restraint (13% to 22%), and the medial retinaculum and MPTL providing lesser amounts. In order to further understand soft tissue restraint throughout the range of knee motion, Nomura et al. (2000) compared restraint provided by the MPFL and medial retinaculum from 20 to 90 degrees of flexion. The results demonstrated that the MPFL continued to

play a larger role than the medial reticulum throughout knee flexion. More recently, a study by Phillopot et al. (2011) examined the roles of the MPFL, MPTL, and MPML throughout knee flexion and found that MPFL provides the greatest amount of restraint in full extension and decreases with knee flexion. This finding is in agreement with the assessment by Amis (2003) that the medial and lateral patellofemoral ligaments slacken as the knee flexes. In contrast, Philippot reported that the percentage of restraint provided by the MPTL and MPML was shown to increase with knee flexion.

In a study by Senavongse and Amis (2005), the roles of all three types of stabilizers were evaluated. Four conditions were tested on cadaveric knees: all structures intact, VMO relaxed (muscle stabilizers), flat trochlea (articular stabilizer), and ruptured medial retinaculum which included the MPFL (passive stabilizers). PF stability was tested by displacing the patella laterally by 10 mm and measuring the reaction force. With a flat trochlea, the force required to displace the patella dropped by 70% at 20 degrees flexion. Rupturing the MPFL caused a significant reduction in restraining force from 0 to 20 degree flexion. The VMO had a significant effect on stability, but contributed the least among the structures that were analyzed, especially in full extension (14%). The study also found that the intact knee reached its lowest amount of PF stability from 20 to 30 degrees flexion. A previous study by the same author demonstrated that lateral PF stability of an intact knee increased with knee flexion from 0 to 90 degrees (Sevavongse et al. 2003). However this result only applied when the patella was displaced by 1 mm, 4 mm, or 7 mm. When the displacement was increased to 10 mm, the least amount of stability occurred at 20 degrees flexion, which corresponds to the results from the previous study.

The literature is sparse in terms of data that demonstrates the influence of the lateral retinaculum's structures on PF stability. However, Desio et al. (1998) included the lateral retinaculum in the selective cutting study that tested resistance to lateral displacement and found that the lateral retinaculum provided on average 10% of the total force. Merican and Amis (2009) examined the influence of the IT band, which is connected to the patella via the IT band-patella fibers, on patella kinematics. They discovered that increasing the IT band force caused the patella to shift and tilt laterally. The previously mentioned studies by Senavongse et al. (2003 and 2005) tested the medial displacement of the patella as well as the lateral. In both studies the results showed that the patella was more resistant to medial displacement than lateral and that the medial resistance increased with knee flexion. Senavongse noted that the lower lateral resistance is likely due to the angle of the muscle force (i.e. Q-angle), which pulls in laterally oriented direction.

Another method of gaining insight into the influence of anatomy on PF stability is to examine the causes of PF subluxation. The literature is in agreement that the main PF subluxation risk factors for the natural knee are patella alta and trochlear dysplasia (Fithian et al. 2001). Yamada et al. (2007) investigated the morphological differences of femoral trochlea for patients with normal PF joints versus patients with recurrent dislocation using three-dimensional models. They evaluated the extent of the "trochlear bump", which is described in terms of the convexity of the trochlea. The results indicated that extent of the convex regions were significantly larger in dislocating knees than in normal knees. Also, the superior border was extended significantly more proximal for the dislocating knees. The researchers hypothesize that proximally-

distributed trochlear grooves exist to accommodate for high-riding patellae. In patients with patella alta, the patella tends to ride on the femoral shaft for a longer distance, which delays the containment of the patella in the trochlear groove and thereby increases the risk of patella dislocation. For the normal knee, the patella engages the trochlear groove at 20 degrees of knee flexion on average (Amis et al. 2006), which is prior to significant decrease in MPFL restraint (Senavongse and Amis 2005).

This body of research suggests that a "hand off" occurs between the passive and the articular stabilizers around 20 to 30 degrees of knee flexion. Multiple studies have confirmed the importance of the MPFL from 0 to 20 degrees of knee flexion (Conlan et al, Desio et al, Philippot et al, Senavongse and Amis). As noted previously, it has also been shown that the patella engages the trochlear at approximately 20 degrees of knee flexion (Amis et al. 2006). Nomura et al. reported in their selective cutting study that that no significant difference was found between the isolated medial retinaculum and MPFL sections at 120 degrees. They noted that the result may be indicative of a larger contribution provided by the articular geometry in deep flexion.

Current State of the Art for Computational Modeling of the PF Joint

Computational models of the PF joint have been developed and employed to accomplish various objectives such as investigating joint forces, contact mechanics, and/or kinematics. Baldwin et al. (2009) developed a subject specific finite element (FE) model based on the experimental data from a deep knee bend activity in the Kansas Knee simulator (KKS). The KKS is a force driven, dynamic simulator that allows full 6

degrees of freedom (DOF) for both the tibiofemoral (TF) and patellofemoral joint (Maletsky and Hillberry 2005). For the purposes of predicting PF kinematics without confounding factors of the TF joint, Baldwin et al. chose to model an isolated PF joint with prescribed TF kinematics. The model included subject specific bone and cartilage surfaces that were extracted from MR images. Soft-tissues were represented using a fiber reinforced composite material model, which consisted of non-linear springs embedded into a two-dimensional (2D) membrane element. The model included representation for the patella tendon, rectus femoris, vastus intermedius, and PF ligaments (Figure 1.4). Baldwin et al. adjusted the ligaments pre-tension values to minimize the difference between the model predicted kinematics and experimental results. Sensitivity analyses were conducted to determine the influence of the PF ligaments' pre-tension and stiffness on kinematics and accuracy of using rigid representation for articular cartilage. Results of the sensitivity analyses showed that modifying the properties of the PF ligaments had the largest effect on PF flexion, ML rotation, and inferior/superior translation while other DOF's were less affected. Also, the sensitivity analyses verified that the deformable and rigid representations of articular surfaces produced similar results.

In further development of a computational model of the KKS, Baldwin et al. (2012) developed subject specific FE models with full 6 DOF's for both the PF and TF joint (Figure 1.5). The knees modeled for the analysis were previously implanted with a total knee replacement (TKR) and underwent in vitro testing that included the KKS deep knee bend, KKS gait, and TF laxity tests. The initial process in the model's development included sequentially addition of TF ligaments and optimizing their parameters until the kinematic difference between the experimental and model predicted internal/external (IE)

and varus/valgus (VV) laxity tests were sufficiently minimized. After fine-tuning of the ligament parameters, the computational model was then verified by simulating the KKS deep knee bend and gait tests and comparing PF and TF kinematic outputs to experimental results. Optimization of the ligaments also included investigating two types of representation: one-dimensional (1D) spring elements and 2D fiber reinforced membranes. The study showed that both representations resulted in similar results, with the 2D representation showing small improvements. It was also noted that the 1D representation resulted in 40% decrease in computation time.

A study by Lanovaz and Ellis (2009) presented a model of a TKR implanted knee that was developed to simulate an in vitro deep knee bend performed on an Oxford style knee rig. The model included full 6 DOF's for both the PF and TF joints. Model parameters were selected for a screening analysis to quantify their influence on simulator outcomes. Results showed that location of ligament insertion and ligament pre-tension had significant influence on the model predicted kinematics. Also, the authors pointed out that the PF kinematics, especially patellar tilt and spin, were more challenging to replicate in the model than the TF kinematics. They recommend that subject specific models with optimized parameters are needed to more accurately model the knee.

Other noteworthy studies include a series of publications by Elias et al. (2004, 2006, and 2010) that describe subject specific PF computational models developed to investigate the influence of various factors such as Q-angle, MPFL reconstruction, and VMO reconstruction on patellofemoral pressures. The soft-tissues were represented by 1D elements and properties were based on a combination of anatomic measurements from cadavers and mechanical properties reported in the literature. Mesfar and Shirazi-

Adl (2005) developed an FE model to examine the contact mechanics of the natural knee from 0 to 90 degrees of flexion. Similar to the models developed by Elias, the soft-tissues were represented by 1D non-linear springs. Several computational models have been developed (Powers et al. 2006; Caruntu and Hefzy 2004; Dhaher and Khan 2002) to investigate PF reaction forces of the natural knee. None of these studies included structures of the medial or lateral retinacula.

In summary, the majority of computational modeling efforts have focused on replicating normal knee activities, such as a deep knee bend or gait, that result in patella kinematics that occur mostly in the sagittal plane. In vitro experiments have demonstrated that the trochlear groove geometry provides up to 70% of patellar stability (Senavongse and Amis 2005) after 20 degrees of knee flexion. Therefore, current PF models, which do not have validated soft tissue structures, rely mainly on the trochlear groove to determine patella kinematics. The published computational models may be verified against in vitro PF kinematics; however, these models have not fully modeled or verified the unique effect that soft-tissue stabilizers have on patella performance. In order to appropriately characterize the mechanical properties of soft-tissue stabilizers in a computational model, verification against experimental PF laxity data is required. The PF laxity test dislocates the patella out of the trochlear in the medial and lateral directions, and provides data on the full extent of the soft-tissue sleeve's influence on patella stability throughout knee flexion. Review of the published literature reveals that experimentally verified computational model based PF laxity data has not yet been developed.

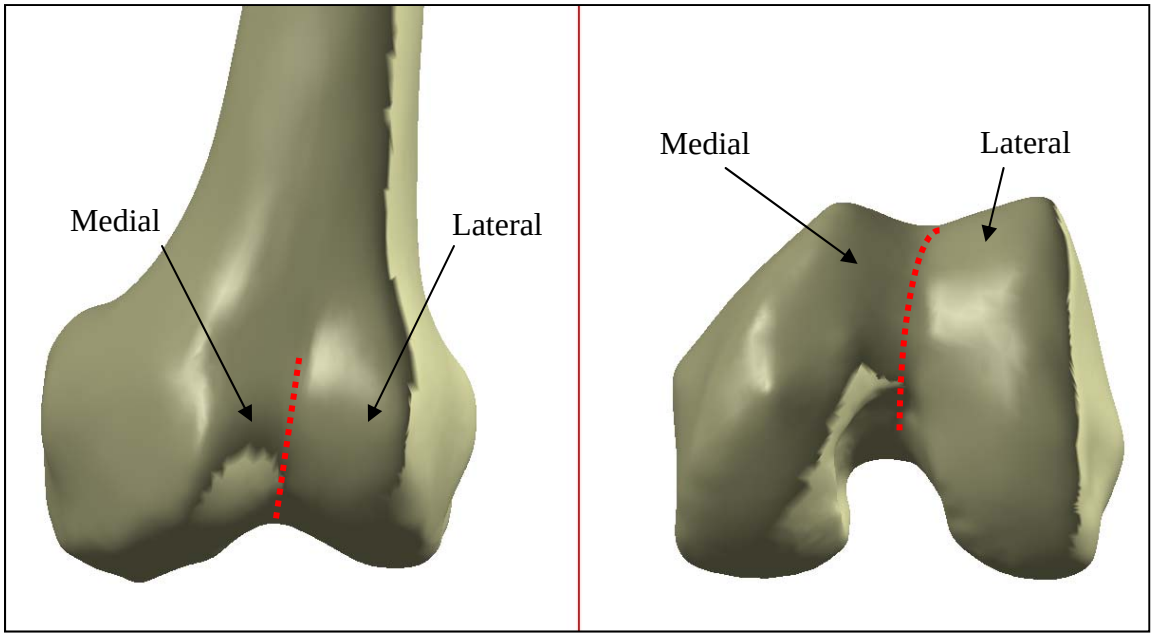

Figure 1.1 Anterior and distal views of the distal femur from a 3D CAD model constructed from a CT scan. Cartilage is not shown. The red dotted line indicates the center of the trochlear groove that is formed between the medial and lateral convex surfaces.

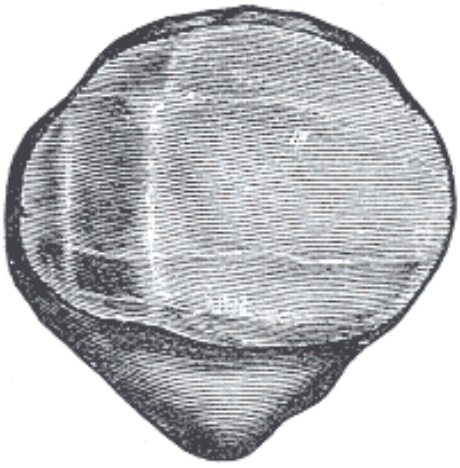

Figure 1.2 Posterior view of the patella, showing facets in the articular cartilage (Gray 1918).

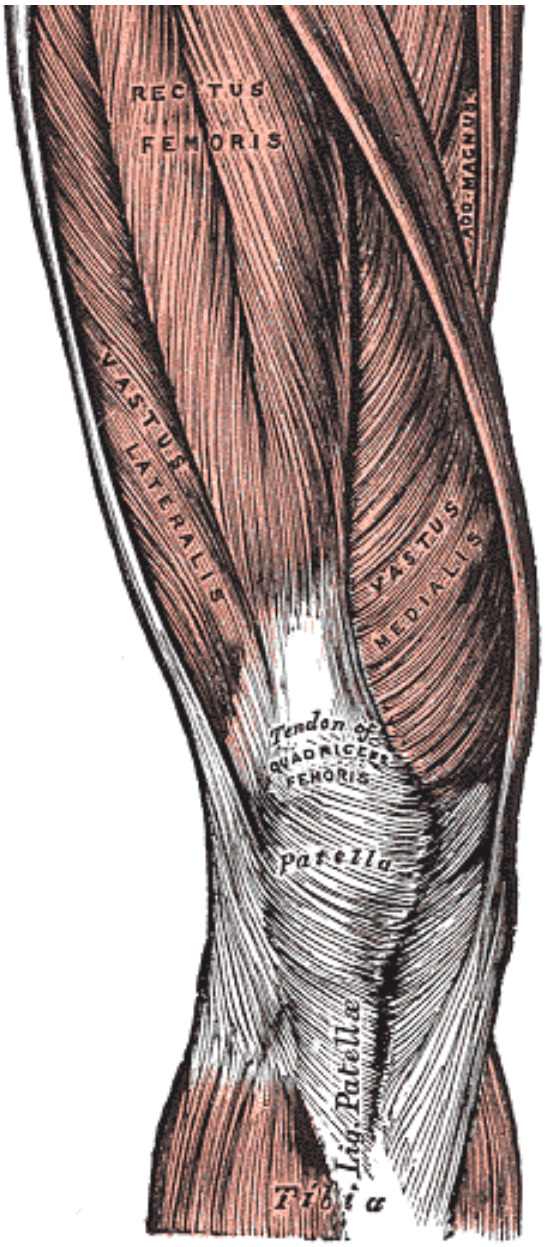

Figure 1.3 Anterior view of the knee, showing three of the muscle groups that form the extensor mechanism (Gray 1918).

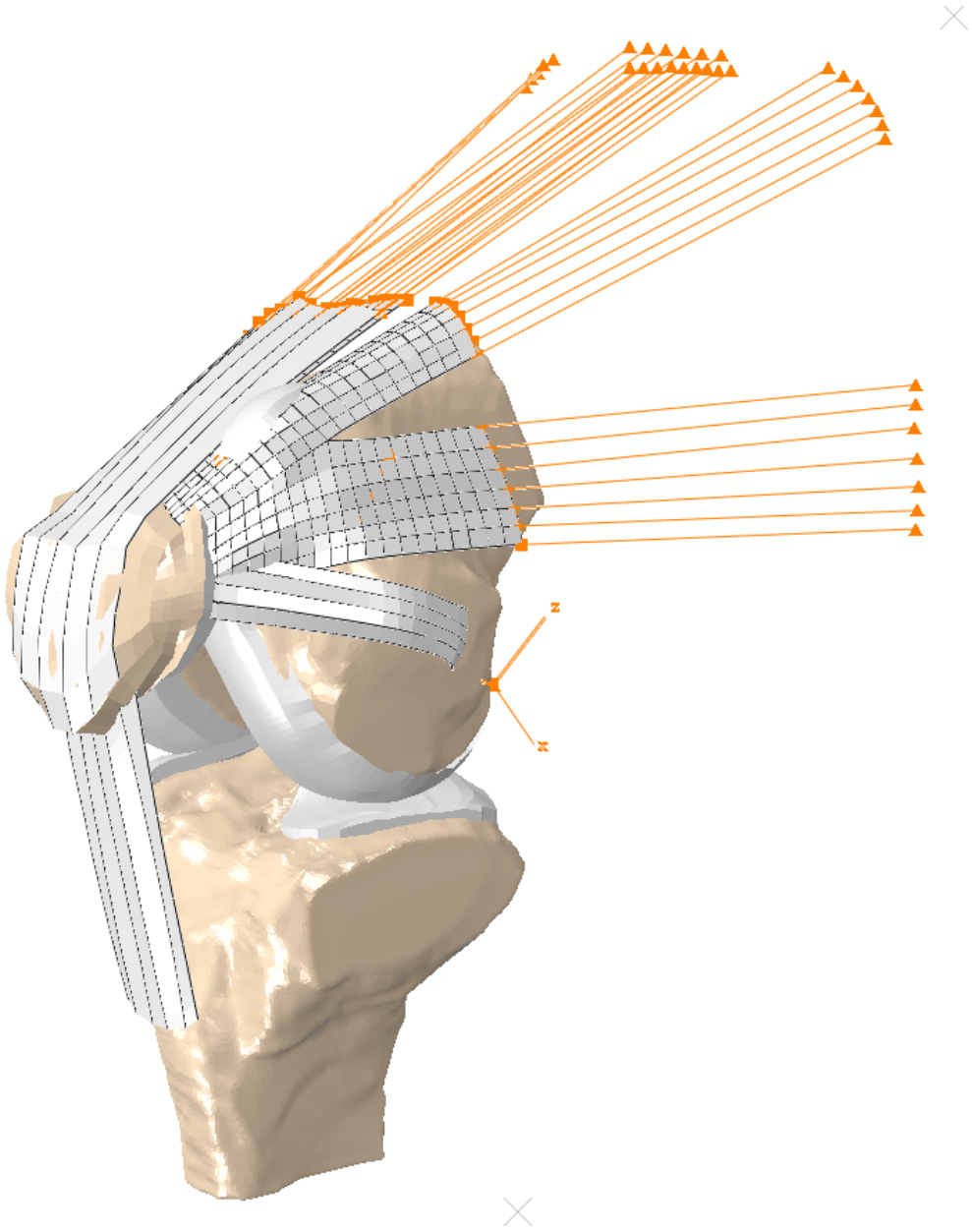

Figure 1.4 Computational model of a natural knee from Baldwin et al. (2009).

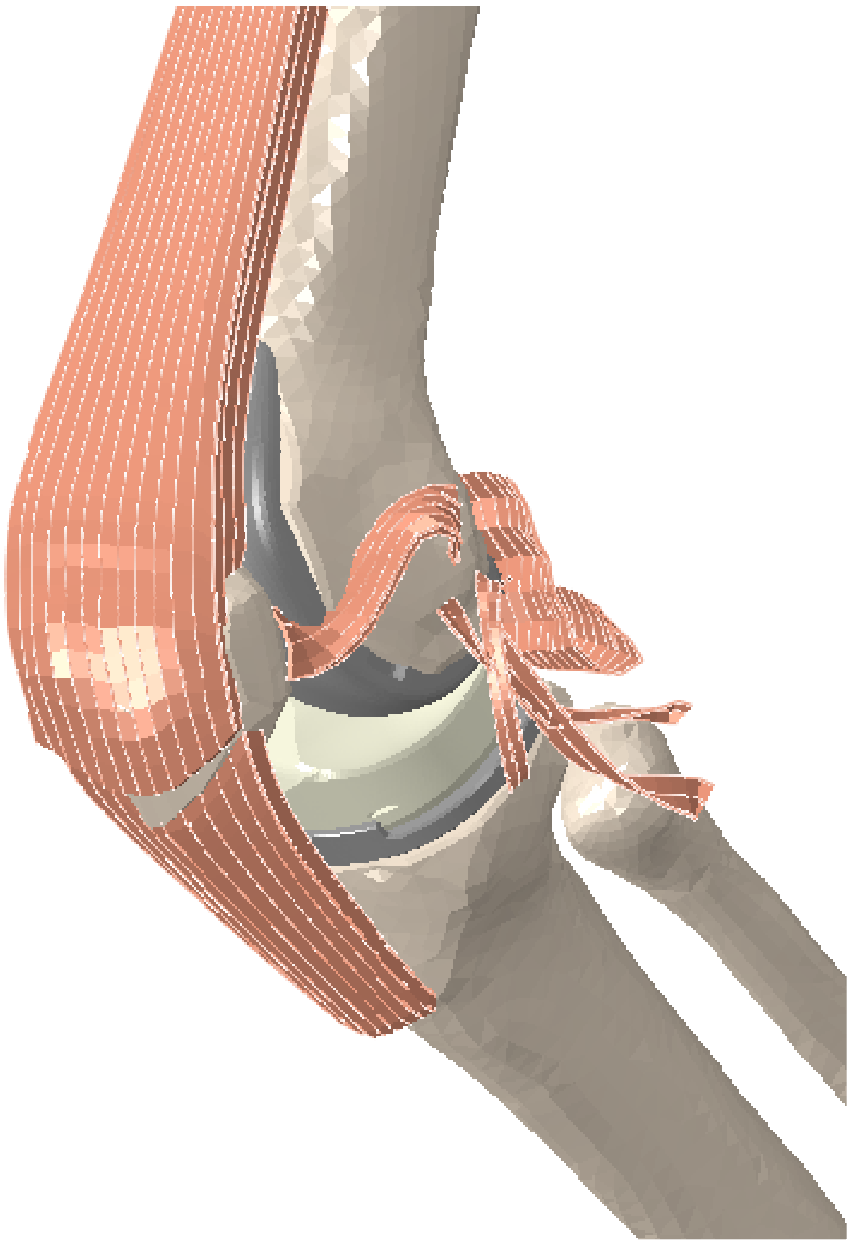

Figure 1.5 Specimen-specific implanted model with 3D extensor mechanism structures and optimized tibiofemoral ligaments.

CHAPTER TWO: METHOD

Cadaveric PF Laxity Experiments

The origins of a new PF computational model with appropriately verified soft-tissue stabilizers are found in PF laxity experimental tests conducted at University of Kansas (Komosa et al. 2011). In these tests, fresh-frozen cadaveric legs were resected 225 mm proximal and 175 mm distal to the epicondylar axis and potted in fixtures. The femoral fixture was rigidly mounted in a muscle loading rig. The rig applied a constant load of 22 N to the rectus femoris and vastus intermedius along the axis of the femoral shaft, while allowing the tibia to be manually flexed and extended. The femur, tibia, and patella were outfitted with motion tracking arrays (Optotrak 3020, Northern Digital Inc., Waterloo, Canada) in order to capture kinematic data. Three experiments were conducted on each specimen through a full range of knee motion: medial patella laxity envelope, lateral patella laxity envelope, and passive range of motion. During such tests, the knee was flexed in approximately 10 degree increments from 0 to 90 degrees and an approximately 44.5 N force was applied to the patella at each increment in either the medial, lateral direction, or neither direction. The force was applied using a custom patella laxity instrument with an integrated load cell to capture load data and a motion tracking array to capture kinematic data (Figure 2.1).

Prior to testing, each specimen was subjected to MR scans in order to capture bony and cartilaginous geometry of the knee. After testing was completed, the knee joint

was dissected and point cloud data of the exterior bone and cartilage geometry was collected by sweeping a stylus attached to a motion tracking array across the articular surfaces of the femur, tibia, and patella. Also, the experiment was repeated after implantation of a total knee replacement by a skilled surgeon. The locations of the femoral component, tibial insert, and patella component relative to the rigid bodies were recorded via the Optotrak motion capture system.

Post-processing of Experimental Data

Post-processing of the PF laxity experimental data followed similar methodology as described by Baldwin et al. (2012) and Clary (2009). The MR data acquired prior to the PF laxity experiments was segmented and used to build finite element meshes of the bones and cartilage for the femur, tibia, and patella. The meshes were aligned relative to their respective rigid body reference frames by visually fitting the 3D meshes to the probed point clouds taken from the natural geometry. The TKA components were also aligned to landmark points probed during the experiment in order to aid in building local coordinate reference frames. Specific points (Figure 2.2) on the femoral, tibial, and patella components were selected based on their general positions relative to the natural anatomy and were used to define a coordinate system as described by Grood and Suntay (1983) (Figure 2.3). Using the transformation matrices exported from the motion capture system along with a custom Matlab script, the meshes for the femur, patella, tibia, and custom patella laxity instrument were transformed into the local coordinate system of the

femoral component. After all the components were transformed into the new coordinate system, a custom Matlab script was used to calculate the Grood and Suntay patellofemoral and tibiofemoral kinematics.

Selection of Cadaveric Data for use in Computational Model

The PF laxity experiment conducted at University of Kansas was performed on multiple specimens. The data from one specimen was chosen for the purposes of building the computational model. The specimen was selected based on the following criteria: adherence to experimental protocol (per conversations with researchers at University of Kansas), availability of MR data, and the ability to cleanly post-process the data without additional interventions to correct apparent discrepancies.

Per specimen, the PF laxity experiments captured ML laxity data from full extension to 90 degrees of knee flexion in approximately 10 degree increments. It was not computationally practical or necessary to use all the experimental data in the optimization of PF computational model. Therefore, the medial and lateral laxity data from three flexion angles and from one passive range of motion were selected to be used in the optimization analysis. The three flexion angles were strategically chosen to include data points in full extension and early flexion (approximately 20 to 30 degrees) where soft-tissue stabilizers are known to have a larger role in PF stability as described in Chapter 1. The remaining flexion angle was specifically chosen at approximately 60 degrees, at a point where influence of the soft-tissues has diminished and the trochlear

groove plays a larger role in PF stability. Plotting the ML patellar translation against knee flexion (Figure 2.4) illustrates the total data available from the PF laxity experiment. For the medial patella envelope analysis, data was selected from tests performed at -3, 22, and 56 degrees of knee flexion. For the lateral patella envelope analysis, data was selected from tests performed at 2, 28 and 61 degrees of knee flexion. For the passive range of motion analysis, data was selected to include a full range of motion from full extension to approximately 90 degrees of flexion.

It should be noted that the protocol from the PF laxity experiment involved manually flexing the tibia and then also manually securing the tibia while the PF laxity data was performed. Because of the manual process, small variations in knee flexion are noted as the patella is translated in the medial and lateral directions (Figure 2.5). Laxity data points with the least variation in knee flexion for were selected for use in optimization of the PF model. The location of the tibial components (in the femoral component reference frame) at the beginning of the medial and lateral laxity experiments were exported and used to prescribe a static location in the computational model.

Using the experimental force and kinematic data from the custom patella laxity instrument, the force vector at each time increment was broken down into the ML, AP, and SI components in the femoral reference frame. The data at 10 points spaced evenly across the time interval was exported for use in the computational model (Figure 2.6).

Visualization of Cadaveric Results

After selection of the cadaveric data was completed, a custom Matlab script was used to create a 3D plot of the motion of the patella relative to the femoral component (Figure 2.7). The visualization of patellar kinematics provided verification that the meshes had been aligned properly to the probed points and that the post-processing of the experimental data had been completed correctly. Minor adjustments were made to the location of the meshes based on the visualization results. Also, after each optimization of the PF computational model, the 3D plots provided an opportunity for visual comparison of experimental and model results.

Computational Model

The PF laxity model was developed to be a subject specific FE model intended to predict the PF kinematics recorded during the PF laxity experiment. To the extent possible, the model inputs, such as bone and cartilage geometry, TF kinematics, and PF reaction loads, were derived from the experiment. Other inputs such as soft-tissue geometry and material parameters were supplied from the literature. The model was isolated to the PF joint in that all six degrees of freedom for the patella were unconstrained while the TF joint had prescribed kinematics. The following sections provide more detail on methods used to create the model.

Bone & Cartilage Representation

The same meshes generated for post-processing of the experimental data were used to represent the bony geometry of the PF model. As mentioned previously, the meshes for the femoral, tibial, and patellar bones were generated from MR scans and used two-dimensional 3-noded triangular elements to represent the outer surfaces of the bones. The meshes for the femoral and patellar cartilage were also generated from the MR scans and represented with three dimensional 8-noded hexagonal elements. The tibial cartilage was not included since the model utilized prescribed TF kinematics. Both the bones and cartilage were modeled as rigid bodies. The femoral and patellar cartilage meshes were rigidly beamed to the rigid body reference nodes of their respective bones' meshes. The contact surfaces between the femoral and patellar assemblies were modeled with the same linear pressure-overclosure relationship used by Baldwin et al. (2009) and Blankevoort et al. (1991).

The meshes for each bone and cartilage assembly were aligned in their respective reference frames using the point clouds that were probed during the experiment. Meshes for the TKA implants were also imported into the assemblies and aligned to probed points. Nodes from the femoral implant that relate to the ML, AP, and SI axes of the component were used to construct a femoral reference frame (Figure 2.2). Nodes from the patella implant that also relate to ML, AP, and SI axes of the patella implant were used to define a reference frame for the natural patella and to track natural patellar

motion throughout the analysis (Figure 2.2). After the femoral, tibial, and patellar assemblies were completed and reference frames established, the assemblies were imported into the femoral reference frame and positioned so that the knee was in full extension. Exported kinematic data was used to choose an initial position for the tibia. Visualization of the patella in the PF laxity experiments was used to obtain an approximate initial position for the patella assembly. The patella was located slightly anterior to the femoral cartilage to prevent initial overclosure of the articular surfaces and to allow for parameter changes during model optimization without causing overclosure.

Soft-tissue Representation

As described in Chapter 1, the muscles and ligaments surrounding the PF joint form a complex network that is partially responsible for providing stability to the patella as it tracks throughout knee flexion. The purpose of the PF computational model was to find the most efficient method of accurately representing patellar kinematics during a PF laxity assessment. Therefore, the overall approach to modeling the soft-tissues was to start with simplistic representations and add complexity as needed. The approach required an iterative process of modeling soft-tissue, running the optimization algorithm, and re-modeling the soft-tissue based on optimization results. Many variations of soft-tissues were investigated, but model development generally followed the pathway listed below.

- Iteration #1: Soft-tissue representation included Rectus Femoris (RF), Patella Tendon (PT), Lateral Patellofemoral Ligament (LPFL), and Medial Patellofemoral Ligament (MPFL) (Figure 2.8)
- Iteration #2: Same as iteration #1 with addition of Lateral Patellomeniscal Ligament (LPML) and Medial Patellomeniscal Ligament (MPFL) (Figure 2.9)
- Iteration #3: Same as iteration #2 with addition of medial and lateral retinacular capsule (Figure 2.10)

These soft-tissue iterations represent milestones of discovery and learning during the development process, and, therefore, their results have been selected for documentation.

The first iteration of soft-tissue representation initially utilized tension only springs to model the RF, PT, LPFL, and MPFL. However, after running several preliminary patella laxity simulations, it was soon discovered that ligament wrapping on the femoral component would be required for stable patella motion. Two-dimensional low modulus, hyperelastic deformable membrane elements were added to the portions of the quadriceps, LPFL, and MPFL in close proximity to the patella for contact with the femur. Tension only springs were embedded into the LFPL and MPFL for fiber reinforcement. The material behavior assigned to the ligaments was based on literature reported experimental force-displacement results for the patellofemoral and quadriceps ligaments responses (Atkinson et al. 2000, Staubli et al. 1999). The location and width of the membranes at their respective patella attachments were based on literature values (LaPrade et al. 2007, Philippot et al. 2009). The ligaments were rigidly attached to the

femur via connector elements. The locations of the PFL's femoral attachments were based on averages reported in the literature (LaPrade et al. 2007), and the orientation of the quadriceps was based on the experimental protocol that aligned the muscle with the anatomic axis of the femur. It should be noted that the other muscle groups of the quadriceps mechanism were not modeled since the majority of the vastus medialis and lateralis muscles were removed during the experiment. The distal portion of the patella was connected to the tibial tubercle with non-linear springs to represent the PT. The location and width of the attachments to the patella and tibia were estimated by examining the MR images. An approximation of the PT's elastic behavior was based on the significantly greater modulus of the PT compared to other ligament structures (Staubli et al.1999).

The second iteration of soft-tissue representation involved the addition of the medial and lateral patellomeniscal ligaments. The PML's were modeled similarly to the PFL's with fiber reinforced membranes at the patella attachment and 2D connected elements at the tibial attachment. The PML's size and attachments were based on literature data (Merican et al. 2007, Dirim et al. 2008, Thawait et al. 2012). However, the literature does not have quantitative landmark location data for the PML's and, therefore, initial placement of these ligaments relied heavily on descriptions and anatomical images shown in the literature.

The final iteration of soft-tissue representation included membranes to represent a capsule around the anterior portion of the knee. The capsule was modeled by bridging the gaps between the quadriceps, PFL, and PML with membrane elements on both the

medial and lateral sides. With the addition of these elements, the soft-tissue model more closely resembled the interconnected network of ligaments that forms the natural retinaculum of the knee.

The following features were modeled as parametric for use in the subsequent optimization analysis, with a total of 35 possible parameters in the final model. Parameter selection was based on initial investigations into the model's sensitivity to perturbations and learning from previously validated FE models (Baldwin et al. 2012).

- Proximal attachment of RF in ML & AP directions
- Distal attachment of PT in ML direction
- Femoral attachments of LPFL & MPFL in AP & SI directions
- Femoral attachment of LPML & LPML in AP & ML directions.
- Lengths of PT, LPFL, MPFL, LPML, MPML
- Stiffness of springs used in the of the composite material for all ligament and capsule representation

It should be noted that the all of the variables that represented a location or length were parameterized by indicating a change from the starting value. For instance, if -5 mm was assigned to the PT length, then the PT would shorten by 5 mm. Or if +5 mm was assigned to the AP location of the RF, then the RF attachment would move 5 mm anterior. The stiffness of the embedded springs was characterized by supplying a maximum force and displacement to define a non-linear force-displacement curve. The force and displacement values were supplied to the model as absolute values.

Boundary Conditions

The dynamic analysis was conducted using Abaqus/Explicit™ 6.11-1 (Abaqus Inc., Providence, RI). The medial and lateral patella laxity simulations were divided into two steps. In the first step, a constant 22 N load was applied to the RF, the tibia was moved into a prescribed location as determined by the experimental kinematic outputs, and adjustments in soft-tissue alignment and material parameters were made. In the second step, the medially or laterally oriented forces recorded by the custom laxity instrument during the experiment were applied to the patella so that the patella was pushed out of the trochlea (Figure 2.6). Individual nodes on both the medial and lateral borders of the patella were chosen as the location for application of the load. These nodes were selected based on their close proximity to the tip of the custom laxity instrument during the experiment. The patella was free to move in all six degrees of freedom, while the tibia and femur were rigidly fixed during the second step.

The passive range of motion (ROM) analysis was also divided into two steps. The first step involved loading the RF with a constant 22 N force and making adjustments in soft-tissue alignment and material parameters. The first step allowed the articular surfaces of the patella and femur to contact and settle into position before flexing the tibia. The tibia was then flexed utilizing kinematic data exported from the experiment.

Each simulation tracked the x, y, and z coordinates of the three patellar tracking nodes during the second step of the analysis and exported the coordinate data for

comparison to experimental data. The method of tracking the patella with the coordinates of three nodes was chosen to eliminate scaling differences that would have existed with different units of measure when tracking the translations and rotations of one node. This allowed only translations, and hence only the unit of millimeters, to be used in the objective function instead of mixing the units of millimeters for translations and degrees for rotations.

Optimization Analysis

Due to the large number of parameters included in the optimization analysis, a series of steps were conducted to explore the design space and assign appropriate initial values to the parameters prior to conducting a comprehensive optimization with all seven of the PF laxity models.

The first step was to explore the design space using the Latin Hypercube DOE technique, which assigns random levels to the parameters within specified bounds. The automation software, Isight 5.6-1 (Simulia. Providence, RI), was utilized to interface with the FE solver and compare model and experimental results. DOE and further optimization were conducted using built-in capabilities available with Isight. Table 2.1 shows the upper and lower bounds that were selected for the parameters included in the initial DOE. The bounds are not absolute values, but instead are relative differences from the starting value of each parameter. The analysis output was the sum of the squared

difference to measure the error between the model and experiment for each tracking node throughout each PF laxity simulation.

Table 2.1 Parameters' upper and lower bounds in the initial DOE

Parameter	Lower Bound	Upper Bound
Rectus Femoris Attachment ML	-10	10
Rectus Femoris Attachment AP	-10	10
Patella Tendon Attachment ML	-10	10
Patella Tendon Length	-10	10
LPFL AP	-10	10
LPFL SI	-10	10
LPFL Length	-10	10
MPFL AP	-10	10
MPFL SI	-10	10
MPFL Length	-10	10
LPFL Max Displacement	-10	10
LPFL Max Force	-50	50
MPFL Max Displacement	-10	10
MPFL Max Force	-50	50

After preliminary exploration of the design space, the passive ROM simulation was used to isolate and optimize the following variables that most affected the extensor mechanism and articular geometry.

- AP & ML position of the RF
- ML and AP position and length of the PT
- AP, MP, & SI position of the patellar and femoral cartilage

Unlike the medial and lateral patella laxity tests, in the passive ROM test the patella is not forced out of the trochlear groove, and therefore, patella kinematics are determined mainly by the extensor mechanism and patellofemoral articular geometry.

Initial investigation involved repeatedly running the passive ROM analysis while varying one factor at a time (OFAT). The OFAT method was utilized to determine appropriate values for the cartilage location and AP position of the PT's tibial attachment. These parameters were not included in later optimization analyses. Also, the lengths of the PFL's and, if present, the PML's were intentionally increased at this stage to ensure that they would have minimal affect on patellar kinematics.

Optimization of the remaining parameters was conducted via the "Pointer" technique built into Isight. The Pointer optimization technique is described as an automatic optimization engine that utilizes a complimentary set of algorithms: a genetic algorithm, Nelder and Mead downhill simplex, sequential quadratic programming (SQP), and a linear solver. One or all of the algorithms may be used by the Pointer technique and are selectively chosen based on their success in finding a solution. The starting values of the parameters, which were chosen based on previous DOE results, and their respective bounds are shown in Table 2.1. The objective function was defined as the minimization of the sum of the squared differences between the model and experiment kinematic results.

Table 2.2 Parameters with starting values and bounds used in Passive ROM optimization

Parameter	Lower Bound	Starting Value	Upper Bound
Rectus Femoris ML	-15.00	-4.63	15.00
Rectus Femoris AP	5.00	11.15	29.23
Patella Tendon ML	0.00	8.23	12.00
Patella Tendon Length	-8.00	-4.43	2.00

With the extensor mechanism parameters optimized, analyses were conducted to fine tune the properties of the remaining ligaments. Initially, the optimization set-up included all seven PF laxity models: three medial simulations, three lateral simulations, and the passive ROM simulations. Several Pointer analyses were conducted with each iteration of soft-tissue representation. Table 2.3 shows the parameters with upper and lower bounds that were included in the comprehensive optimization analysis for the final soft-tissue representation. Please note for this analysis that the maximum force values for the embedded springs were removed to reduce the number of parameters included in the analysis.

Table 2.3 Parameters included in optimization for final soft-tissue representation

Parameter Name	**Lower Bound**	**Starting Value**	**Upper Bound**
LPFL Length	-10	7.0516	25
MPFL Length	-20	-4.4633	10
LPFL Attachment SI	-15	-10.275	11
MPFL Attachment SI	-15	0.56212	20.73
LPFL Attachment AP	-8.05	-1.1111	11.95
MPFL Attachment AP	-12.33	9.2773	10
LPML Length	-15	11.88	15
MPML Length	-15	-1.0718	15
LPML Attachment ML	-10	-1.7725	10
MPML Attachment ML	-10	8.9964	10
LPML Attachment AP	-10	0	10
MPML Attachment AP	-10	0	10
LPFL Max Displacement	3	16	40
MPFL Max Displacement	3	35	40
LPML Max Displacement	3	12	40
MPML Max Displacement	3	6	40
Proximal Lateral Capsule Max Displacement	3	4	40
Distal Lateral Capsule Max Displacement	3	30	40

Proximal Medial Capsule Max Displacement	3	23	40
Distal Medial Capsule Max Displacement	3	22	40

After optimizations of the first two iterations of soft-tissue modeling, it was noticed that a substantial portion of the error between the model and experiment was from the medial patella laxity and passive ROM tests. Therefore, in order to determine if the medial PF laxity simulation results could be improved, the analysis was scaled down and Iteration #3 was optimized using only the medial PF laxity and passive ROM simulations.

Post-processing

Upon completion of the optimization routine, all of the PF laxity models were evaluated with the combination of parameters that had the lowest objective function. The coordinates of the three patellar tracking nodes were exported to a text file. A custom Matlab script used the coordinate results to calculate Grood and Suntay kinematics for comparison to the experimental data. The root mean square (RMS) differences between experimental and model predicted kinematics were calculated for all 6 degrees of freedom and the average taken for translations and rotations of each PF laxity model. The overall average for translations and rotations was also calculated for each model iteration.

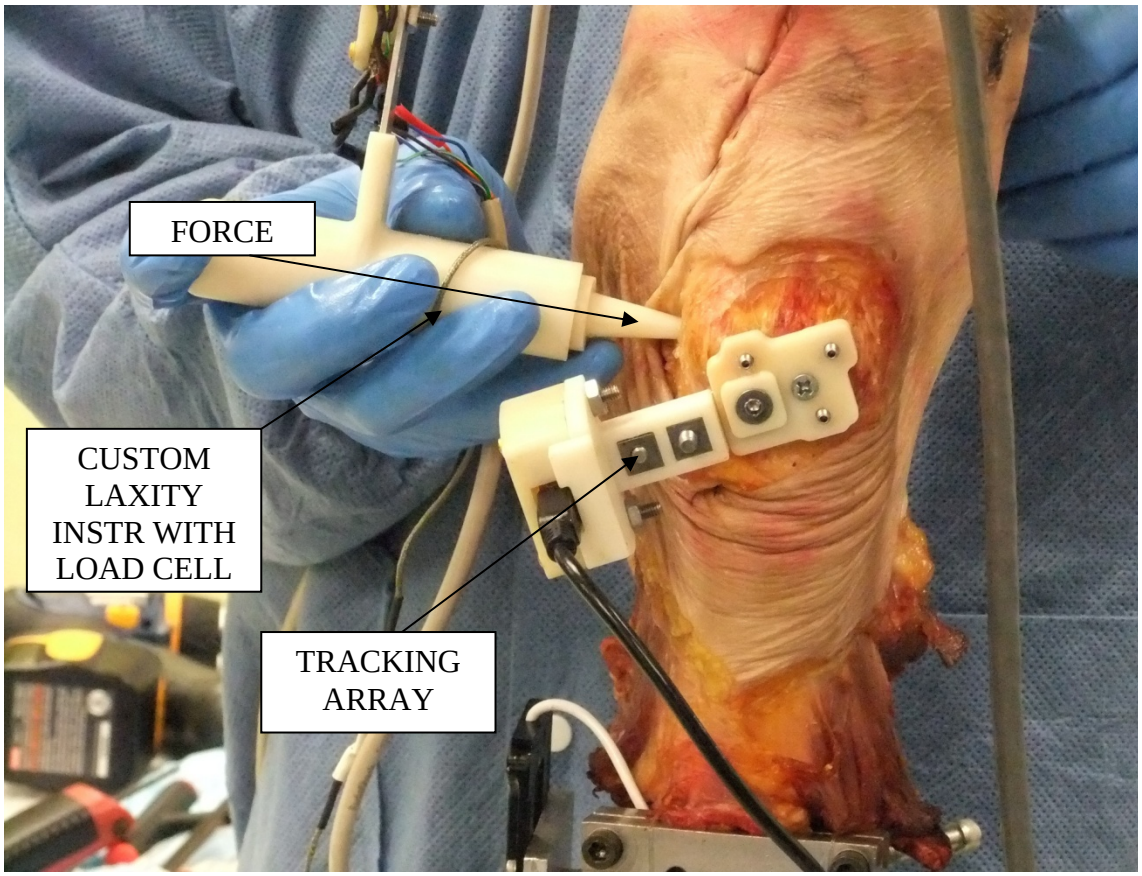

Figure 2.1 Custom patella laxity instrument with an integrated load cell to capture load data and motion tracking arrays to capture instrument and knee kinematics.

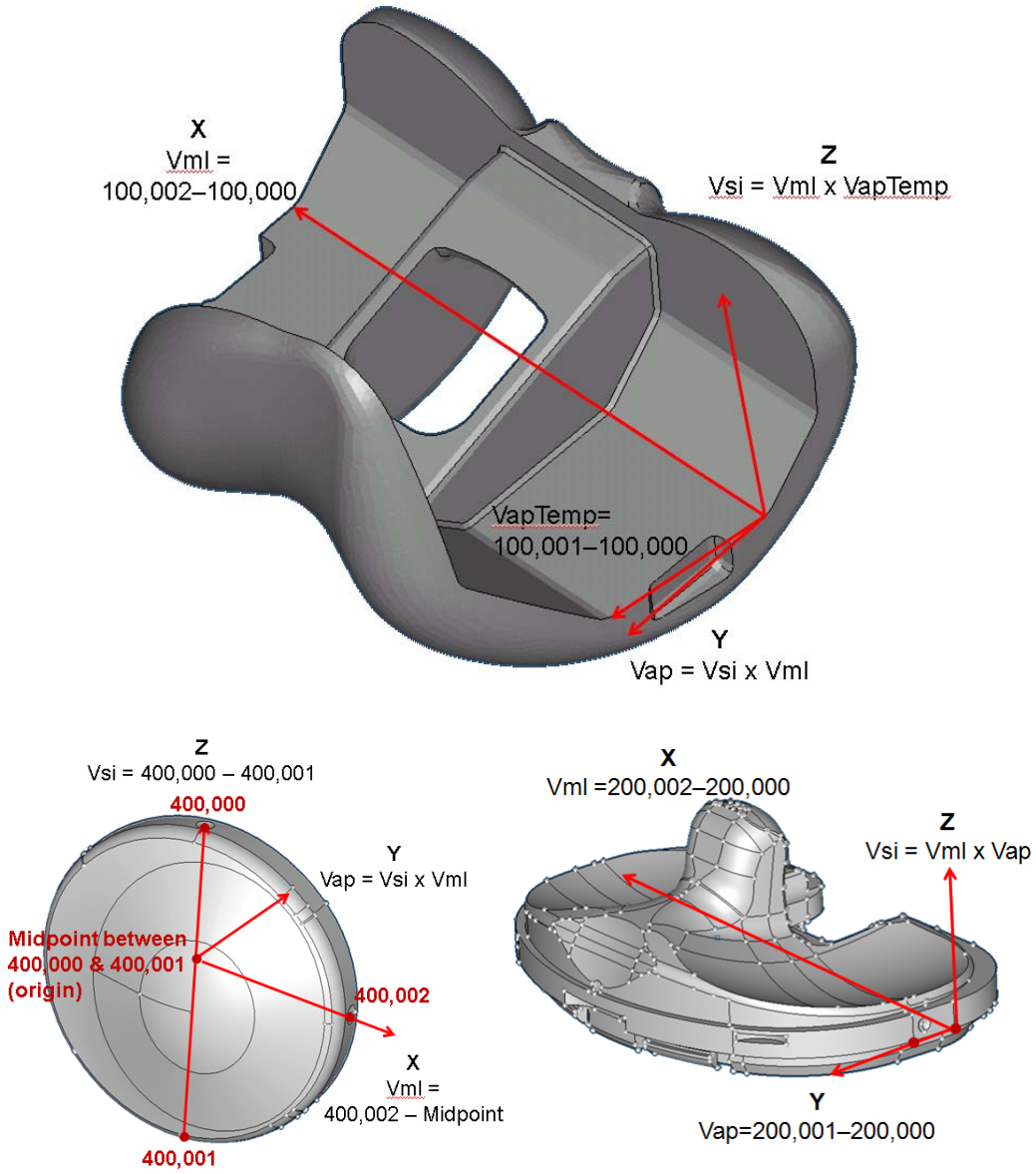

Figure 2.2 Points on the femoral, tibial, patella components were used to define local coordinate systems.

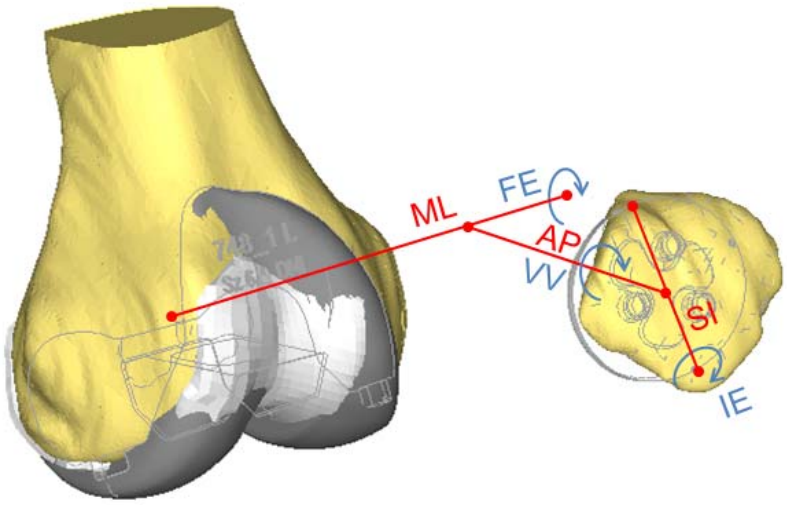

Figure 2.3 Grood & Suntay coordinate system defined for the PF joint. Points on the femoral and patella components were used to build the ML and SI axes.

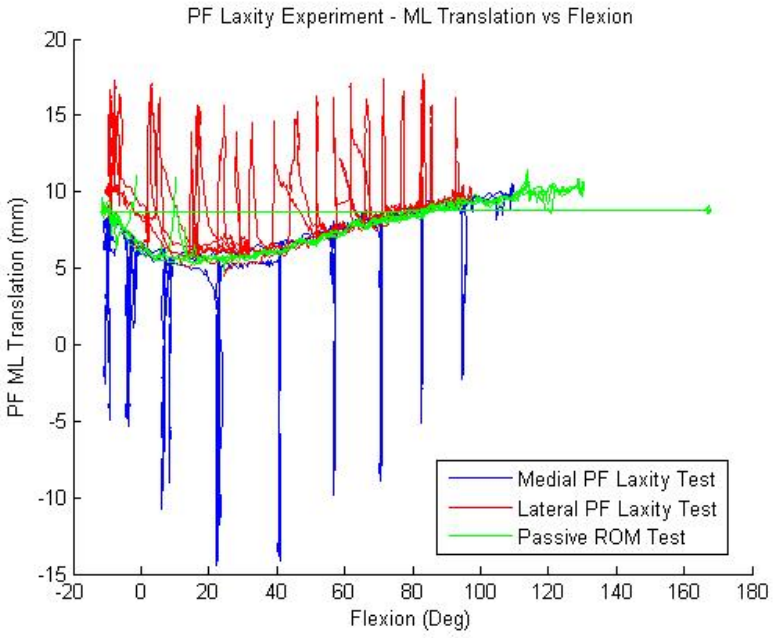

Figure 2.4 ML translation versus knee flexion for the experimental PF laxity tests.

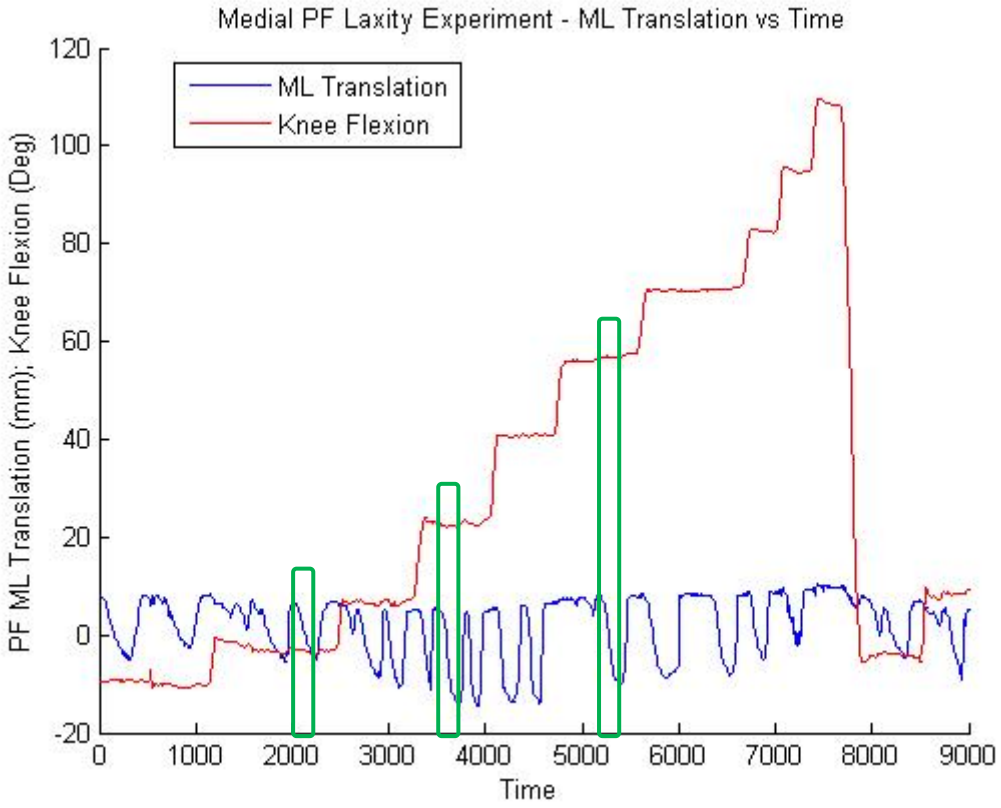

Figure 2.5 ML translation versus time for the experimental medial PF laxity test. Data selected for use in the three medial PF Laxity simulations are indicated by green boxes.

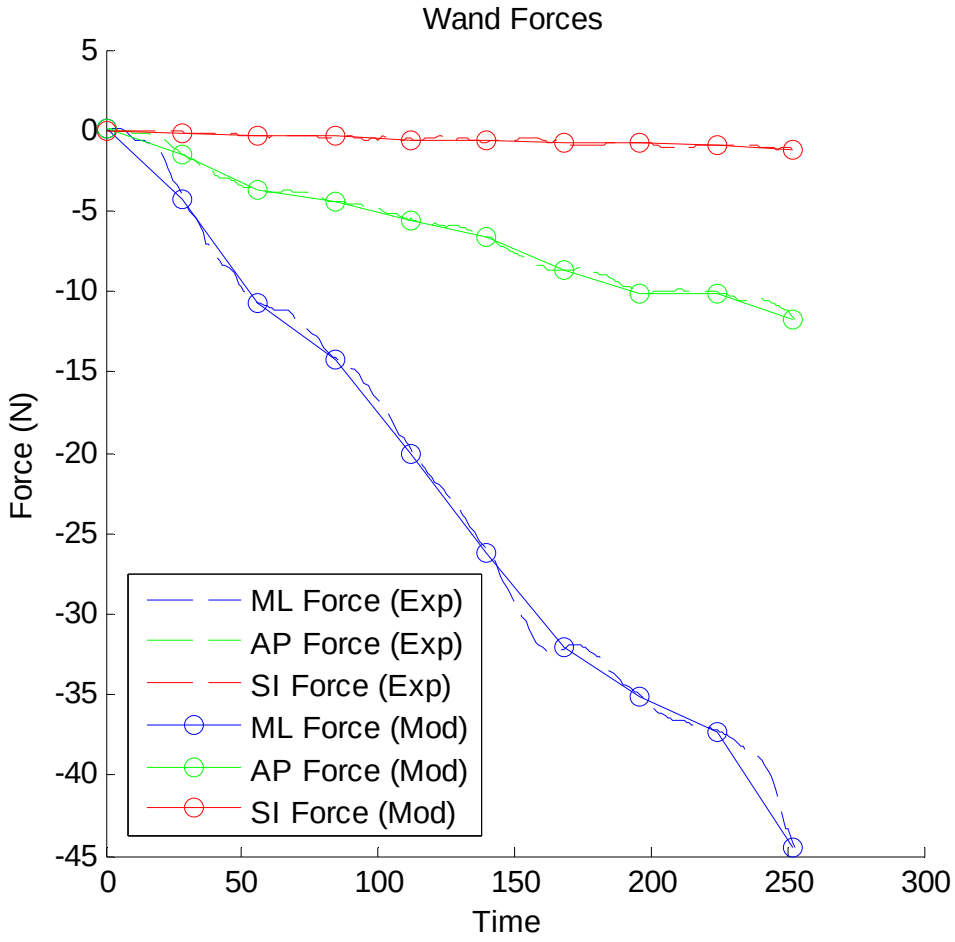

Figure 2.6 ML, AP, and SI force components were calculated from experimental force and kinematic data. Ten evenly spaced points were exported for use in the computational model.

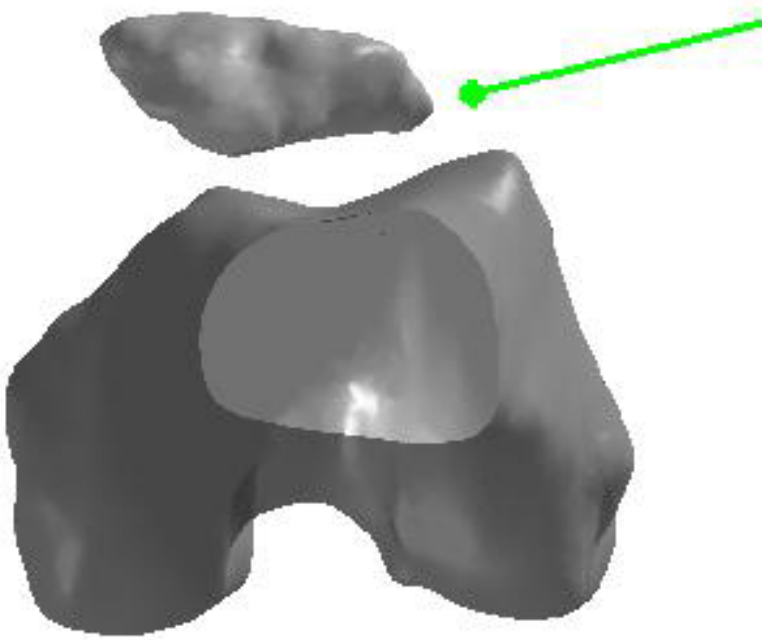

Figure 2.7 Example of 3D plot of patella, femur, and custom PF laxity instrument.

.

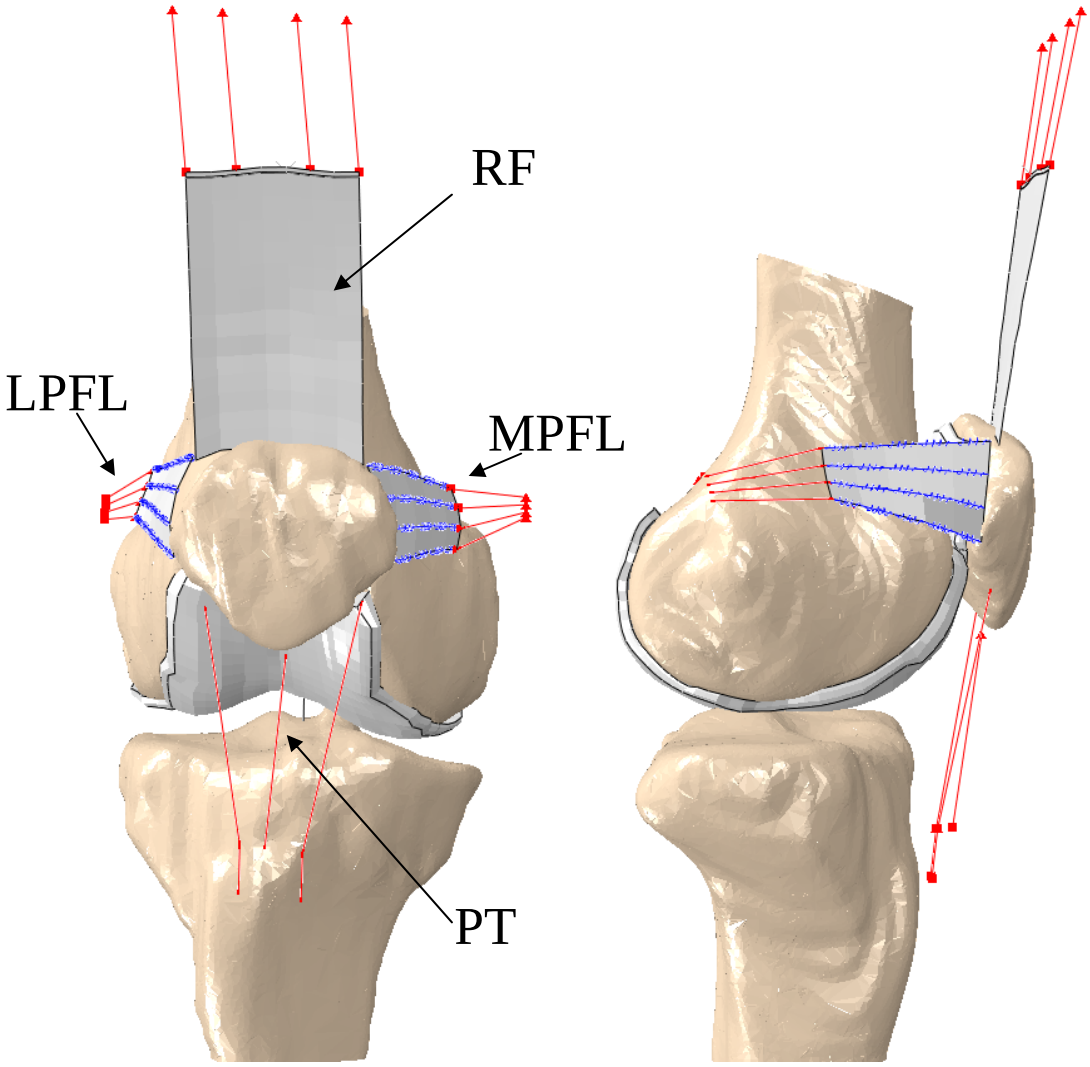

Figure 2.8 Iteration #1 of the PF Laxity Model (front and side views); Soft-tissue representation includes Rectus Femoris (RF), Patella Tendon (PT), Lateral Patellofemoral Ligament (LPFL), and Medial Patellofemoral Ligament (MPFL).

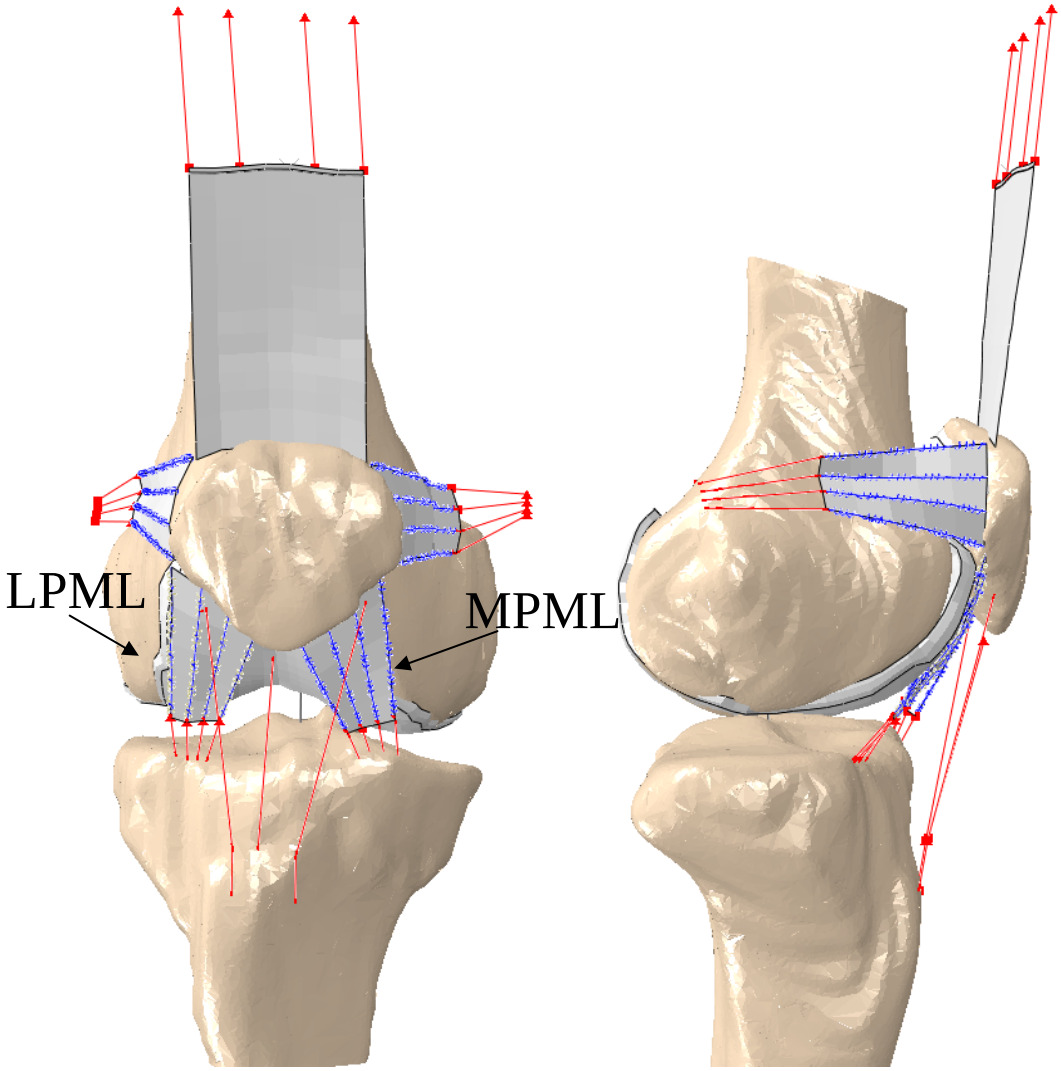

Figure 2.9 Iteration #2 of the PF Laxity Model (front and side views); Soft-tissue representation has same structures as Iteration #1 with addition of Lateral Patellomeniscal Ligament (LPML) and Medial Patellomeniscal Ligament (MPFL).

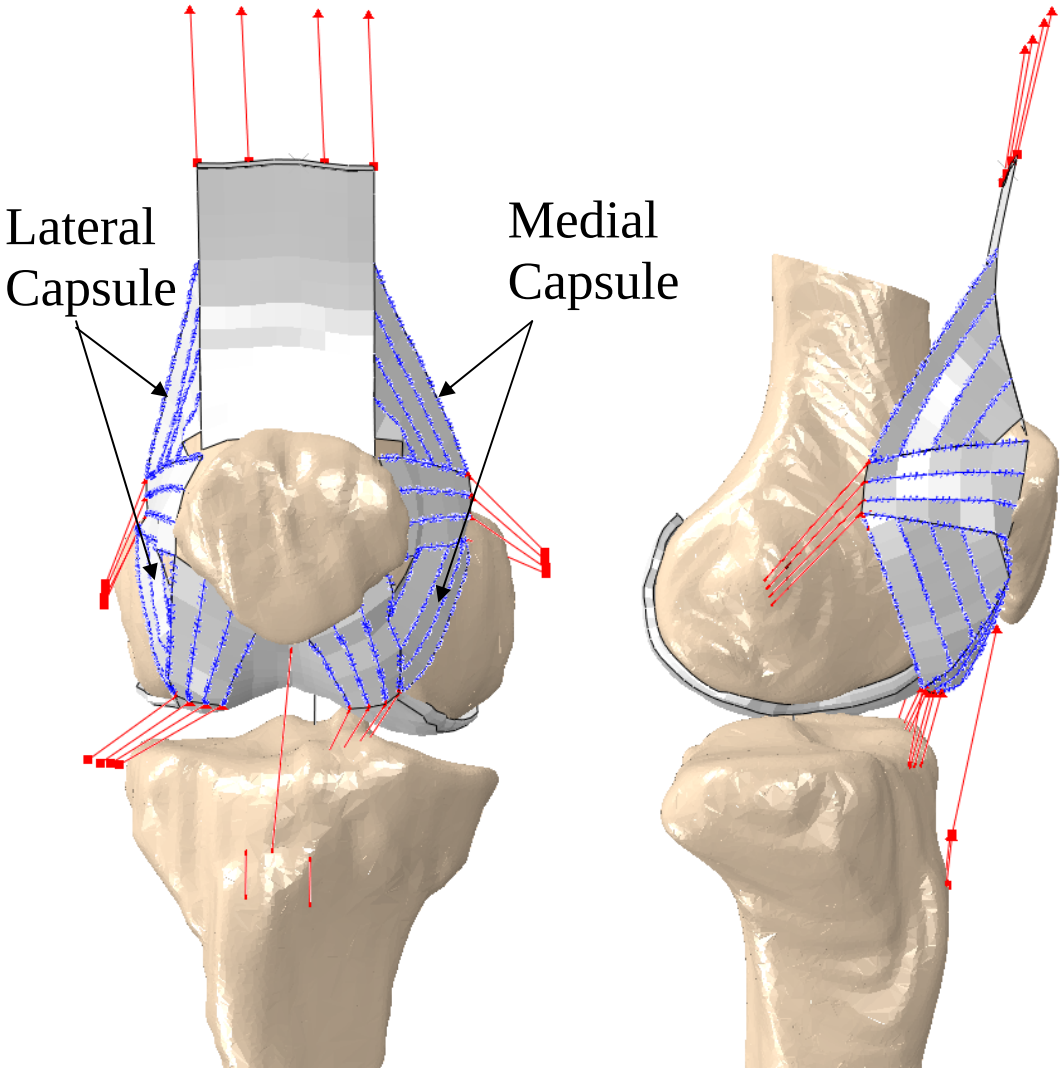

Figure 2.10 Iteration #3 of the PF Laxity Model (front and side views); Soft-tissue representation has same structures as Iteration #2 with addition of medial and lateral retinacular capsule.

CHAPTER THREE: RESULTS

PF Laxity Model Results for Iterations #1 & #2

Objective function results from the optimization of iterations #1 and #2 were similar, with no improvements seen in overall score with the addition of the patellomeniscal ligaments. The minimum objective functions for iterations #1 and #2 were 15110 and 15320, respectively. Nevertheless, the addition of the LMPL and MPML did prevent the patella from becoming unstable and sliding off the femur, which was an issue for Iteration #1 under certain parameters at 60 degrees.

The average RMS results demonstrated similar differences between model predicted and experimental translations for iterations #1 and #2 (Table 3.1). However, in terms rotational differences, the average RMS results improved for a majority of the PF model laxity models and for the overall with iteration #2. The largest improvement of 4.2 degrees was observed at full extension in the Medial PF laxity model.

Table 3.1 Average RMS differences between experimental and model predicted translations and rotations for iterations #1 and #2.

	Average RMS (mm)	
	Iteration #1	**Iteration #2**
Med PF Laxity @ Full Extension	3.4	3.3
Med PF Laxity @ ~25 Degrees	2.6	3.0
Med PF Laxity @ ~60 Degrees	2.8	1.8
Lat PF Laxity @ Full Extension	2.1	2.9

Lat PF Laxity @ ~25 Degrees	1.2	1.6
Lat PF Laxity @ ~60 Degrees	2.5	3.6
Passive ROM	2.1	1.5
Overall Average RMS	**2.4**	**2.5**
	Average RMS (deg)	
	Iteration #1	**Iteration #2**
Med PF Laxity @ Full Extension	10.5	6.3
Med PF Laxity @ ~25 Degrees	4.4	3.3
Med PF Laxity @ ~60 Degrees	5.2	4.0
Lat PF Laxity @ Full Extension	6.4	6.9
Lat PF Laxity @ ~25 Degrees	9.6	9.9
Lat PF Laxity @ ~60 Degrees	8.1	5.5
Passive ROM	2.4	2.3
Overall Average RMS	**6.7**	**5.4**

Figures 3.2- 3.4 illustrate a side-by-side comparison of the kinematic results from the three iterations of the PF laxity models. The ML translation, AP translation, and IE rotation results were chosen for this comparison since they are the components of motion in the coronal plane, where the majority of the motion for PF laxity test occurs. When examining kinematic results from Iteration #1 and #2, it was noticed that substantial differences existed between the model and experiment in terms of ML translation during the medial patella laxity tests, as shown in Figure 3.2. In full extension the patella was translating approximately 10 mm more than in the experiment. At other flexion angles, however, the patella was translating up to 10 mm less than in the experiment. This scenario posed the challenge of adding the appropriate features and/or making changes to the model parameters that would provide more constraint in full extension while providing less constraint in flexion.

PF Laxity Model Results for Iteration #3

The following changes were made to the final iteration of the soft-tissue model in order to make improvements to the ML translation results during the medial laxity tests. First, capsular elements were added between the RF, PFL's, and PML's on both the medial and lateral sides of the knee. Addition of the capsule provided a reduction in medial translation in full extension by ensuring that soft-tissue wrapping would always occur at the most prominent points of the anterior femur (Figure 3.7). Without the capsule, the LPFL tended to articulate proximal to the anterior condyle. Also, in full extension the soft-tissue elements articulated with both the femoral cartilage and bone. The position of the bone relative to the experimental probed points was re-examined, and the bone was translated 1.7 mm anterior and 1.5 mm superior. The change in the location provided additional constraint to the soft-tissue as it wrapped around the bone. The position of the cartilage was not modified.

In order to decrease the amount of constraint provided at the ~25 degree and ~60 degree flexion angles, the patella tendon representation was simplified to a single connector element. It was noted that the combination of multiple connector elements created an over-constrained assembly due to the rigidity of the individual elements. Also, the geometry of the cartilage had square peripheral edges due to the use of brick elements in the mesh. It was hypothesized that these edges were removing slack in the PFL's and PML's in model, and therefore, the edges of the cartilage were modified to smoothly blend into the femoral geometry. Deterministic runs of the model demonstrated that

simplification of the PT representation and modification of the peripheral cartilage allowed the patella to translate further medially in flexion.

Optimization of iteration #3, which only included the medial laxity and passive ROM models, demonstrated an order of magnitude improvement in objective function results compared to iteration #2. The starting objective function was 2099 and decreased to a minimum of 1634 after 103 runs.

The average RMS differences between model predicted and experimental translations decreased to 1.9, 2.1, and 0.7 mm for the medial PF laxity models at full extension, ~25 degrees flexion, and ~60 degrees flexion, respectively (Table 3.1). However, the improvements achieved for the medial PF laxity model were offset by increases in average RMS results for the lateral PF laxity tests. The overall average RMS result for the PF laxity models remained unchanged at 2.5 mm from iteration #2 to iteration #3. Small improvements were observed between iterations #2 and #3 in terms of the average RMS differences between model and experimental rotations, with overall average RMS values of 5.4 and 5.2 degrees, respectively.

The improvements made with the third model iteration are evident in the medial PF laxity results for ML and AP translation and IE rotations (Figures 3.2-3.4). Kinematic results for the remaining DOF's (SI translation, FE rotation, and VV rotation) from iteration #3 are shown in Figure 3.5. The passive ROM kinematic results for all 6 DOF's are shown in Figure 3.6. Visualization of the the final time step from each PF laxity model for iterations #1, #2, and #3 and the corresponding cadaveric experiments are shown in Figures 3.8-3.11.

Table 3.2 Average RMS differences between experimental and model predicted translations and rotations for all three model iterations.

	Average RMS (mm)		
	Iteration #1	**Iteration #2**	**Iteration #3**
Med PF Laxity @ Full Extension	3.4	3.3	1.9
Med PF Laxity @ ~25 Degrees	2.6	3.0	2.1
Med PF Laxity @ ~60 Degrees	2.8	1.8	0.7
Lat PF Laxity @ Full Extension	2.1	2.9	4.3
Lat PF Laxity @ ~25 Degrees	1.2	1.6	3.3
Lat PF Laxity @ ~60 Degrees	2.5	3.6	3.9
Passive ROM	2.1	1.5	1.4
Overall Average RMS	**2.4**	**2.5**	**2.5**
	Average RMS (deg)		
	Iteration #1	**Iteration #2**	**Iteration #3**
Med PF Laxity @ Full Extension	10.5	6.3	6.5
Med PF Laxity @ ~25 Degrees	4.4	3.3	3.8
Med PF Laxity @ ~60 Degrees	5.2	4.0	3.1
Lat PF Laxity @ Full Extension	6.4	6.9	7.0
Lat PF Laxity @ ~25 Degrees	9.6	9.9	8.3
Lat PF Laxity @ ~60 Degrees	8.1	5.5	3.9
Passive ROM	2.4	2.3	3.7
Overall Average RMS	**6.7**	**5.4**	**5.2**

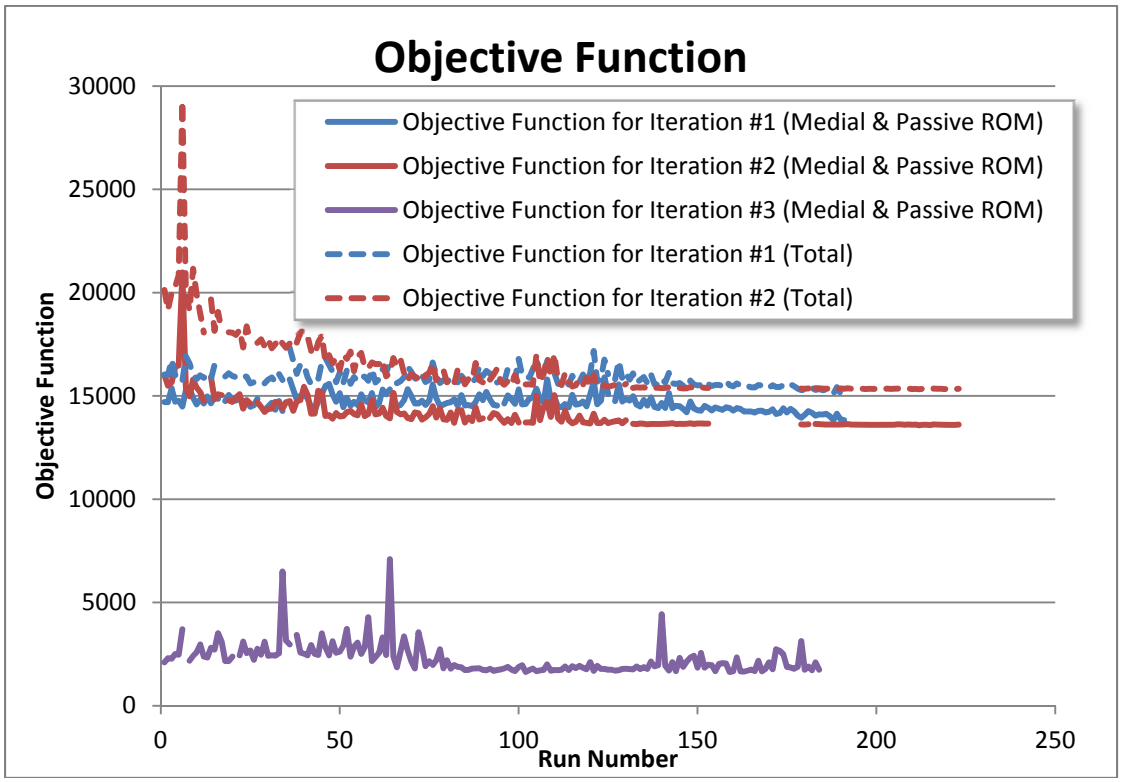

Figure 3.1 Objective function results from optimization analyses of three PF laxity model iterations.

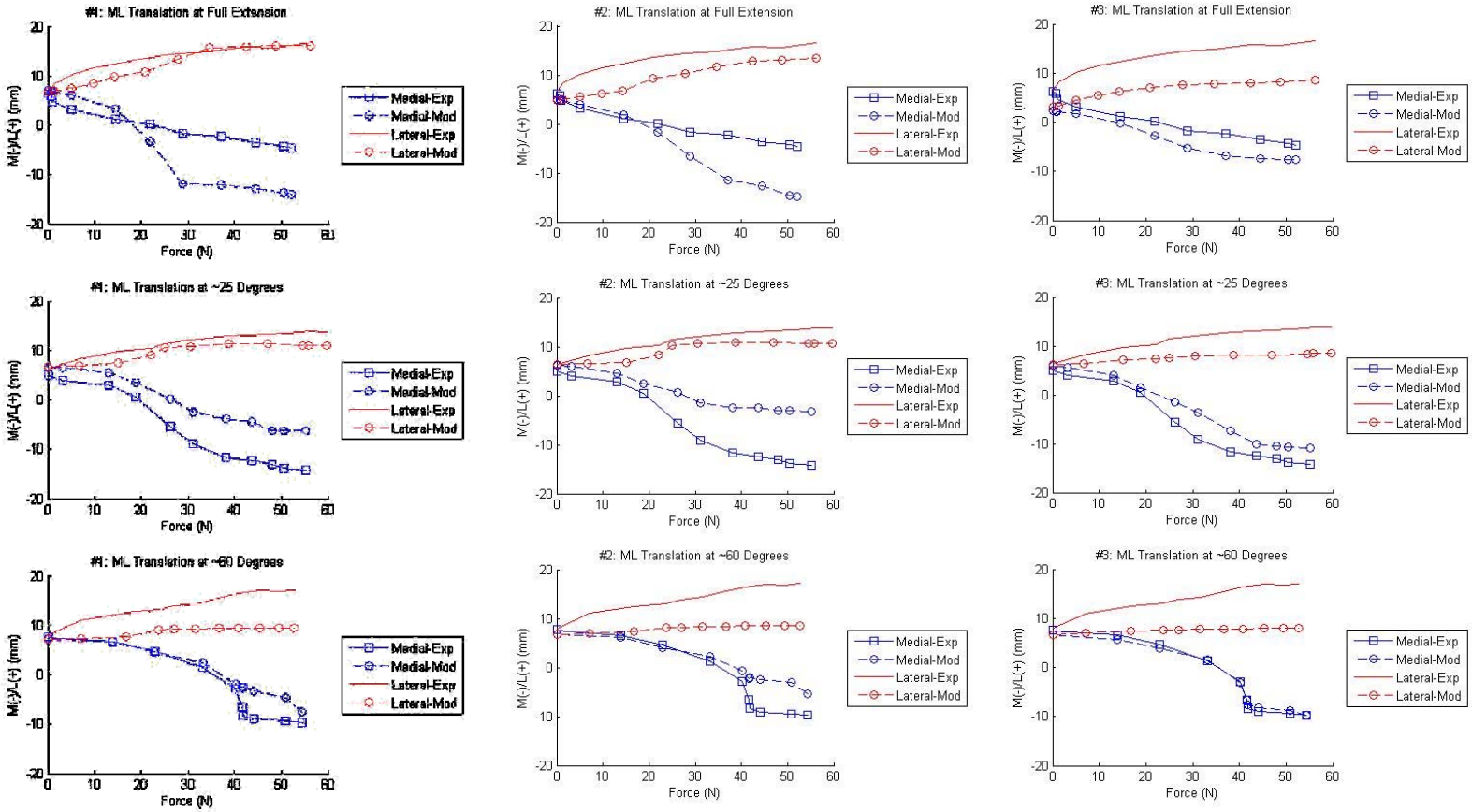

Figure 3.2 ML translation results from experiment and three iterations of PF laxity model.

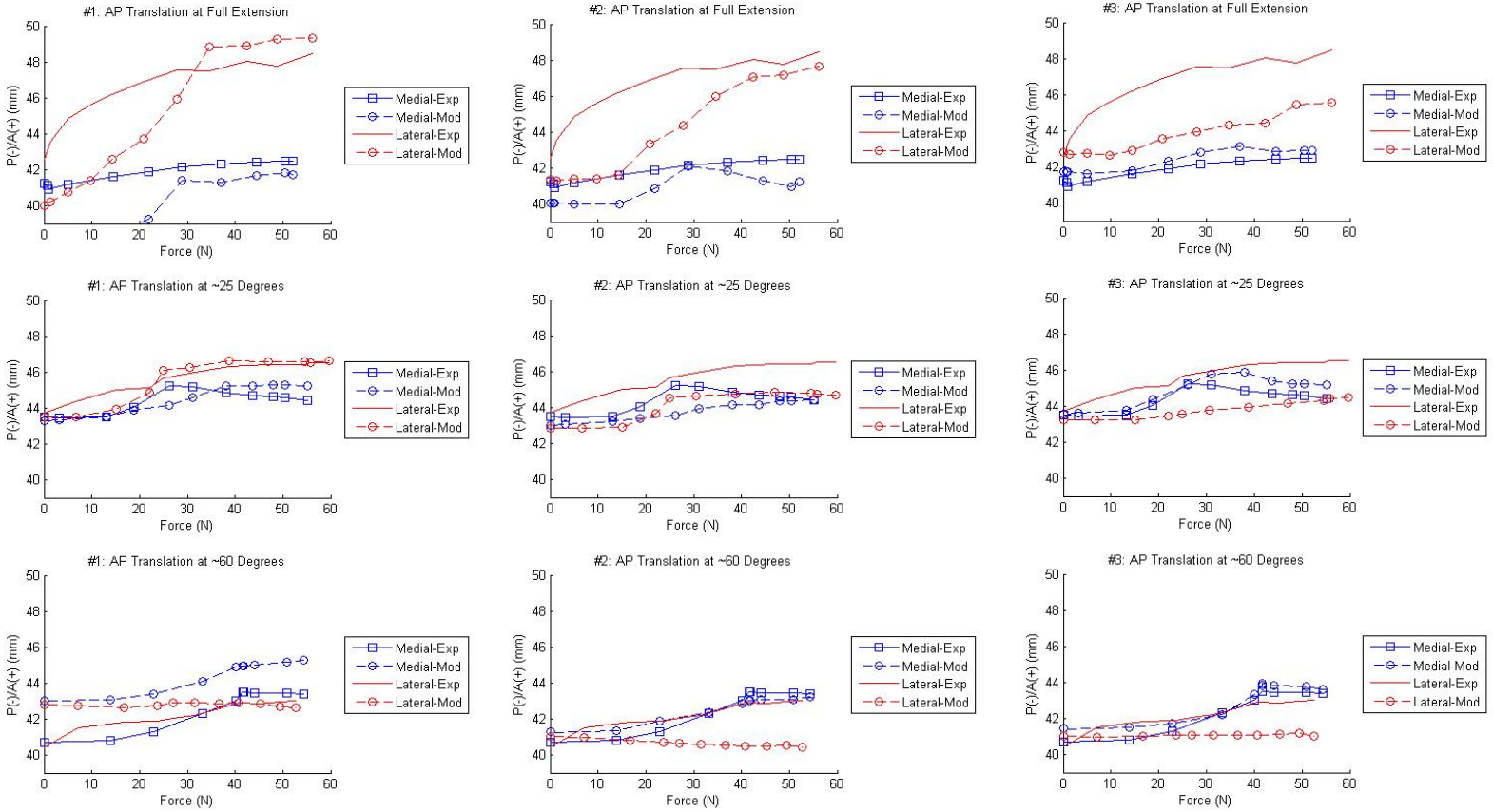

Figure 3.3 AP translation results from experiment and three iterations of PF laxity model.

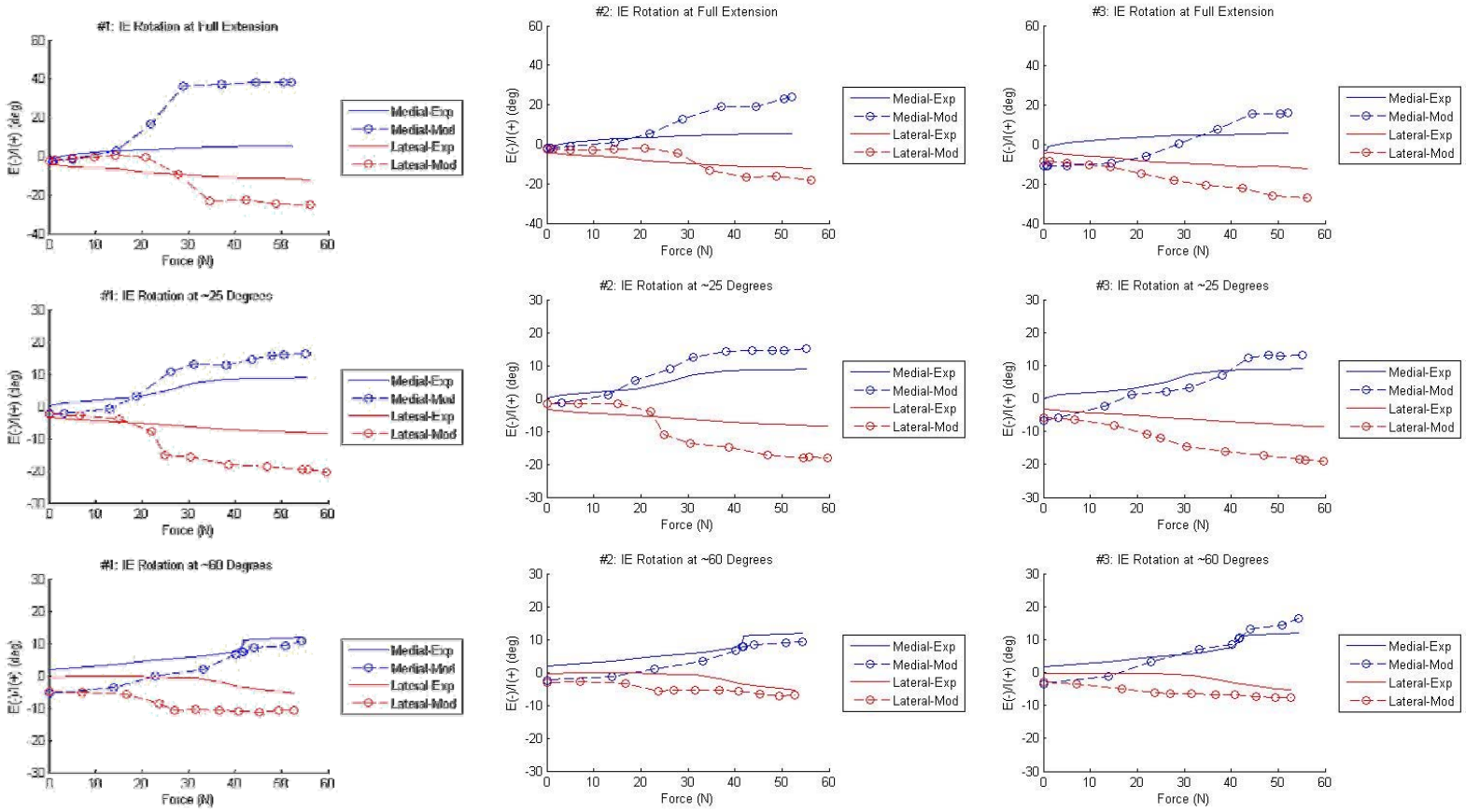

Figure 3.4 IE rotation results from experiment and three iterations of PF laxity model.

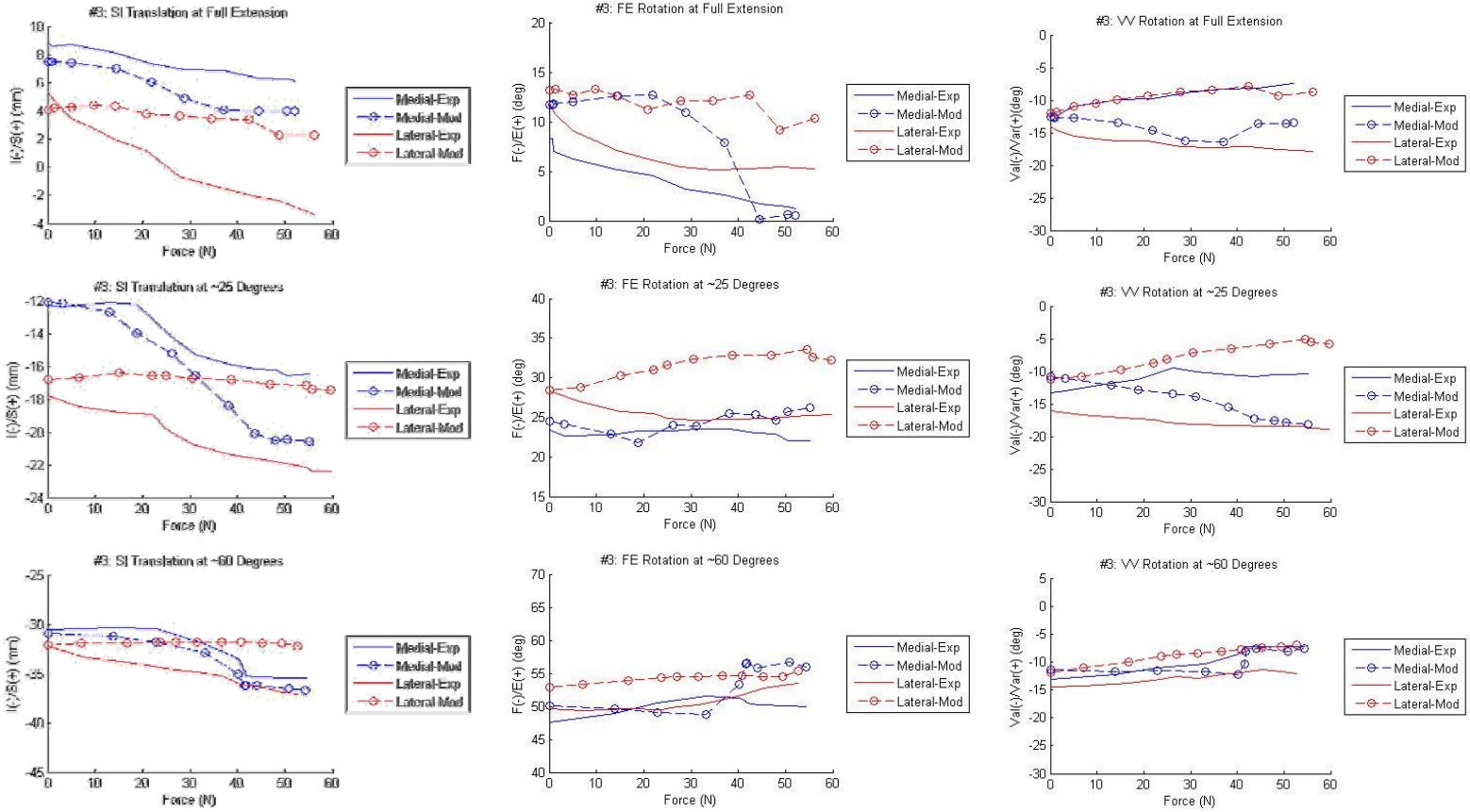

Figure 3.5 SI translation and FE & VV rotation results from experiment and final iteration (#3) of PF laxity model.

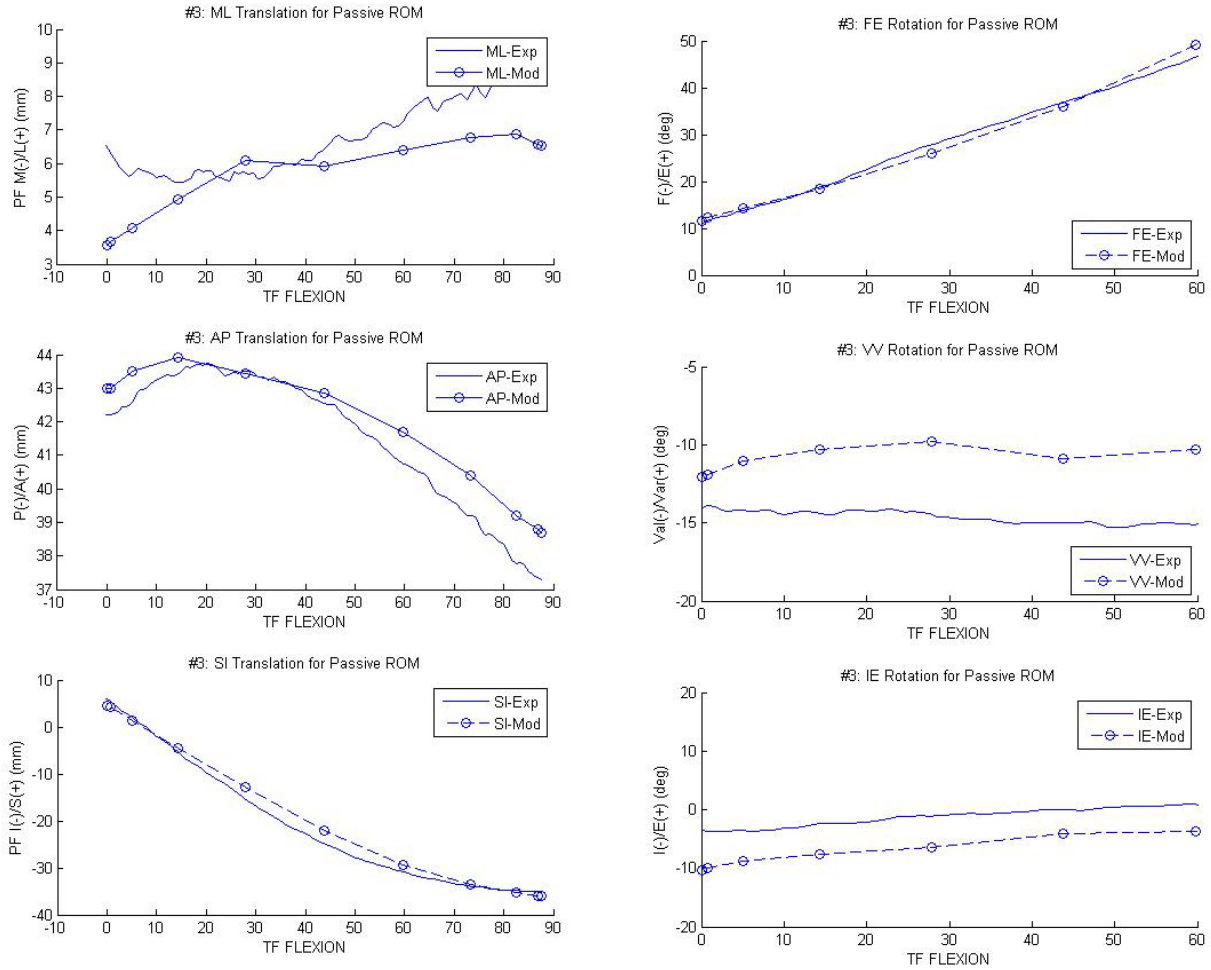

Figure 3.6 Passive ROM kinematic results (6 DOF) from experiment and final iteration (#3) of PF laxity model.

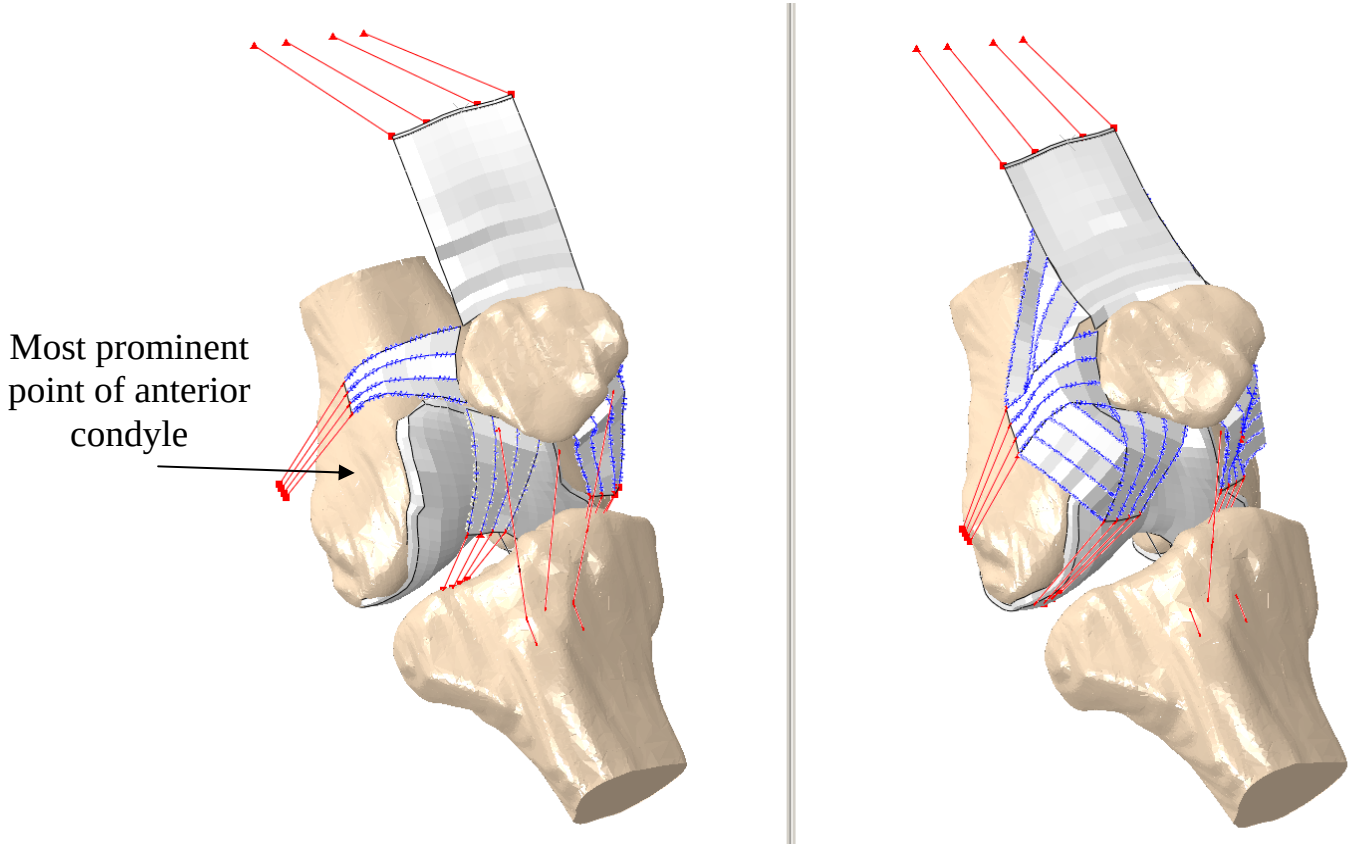

Figure 3.7 In Iteration #2 (left), the LPFL does not contact the most prominent point of the anterior condyle during the medial laxity test in full extension. In Iteration #3 (right), the capsular elements wrap over the most prominent point of the anterior condyle.

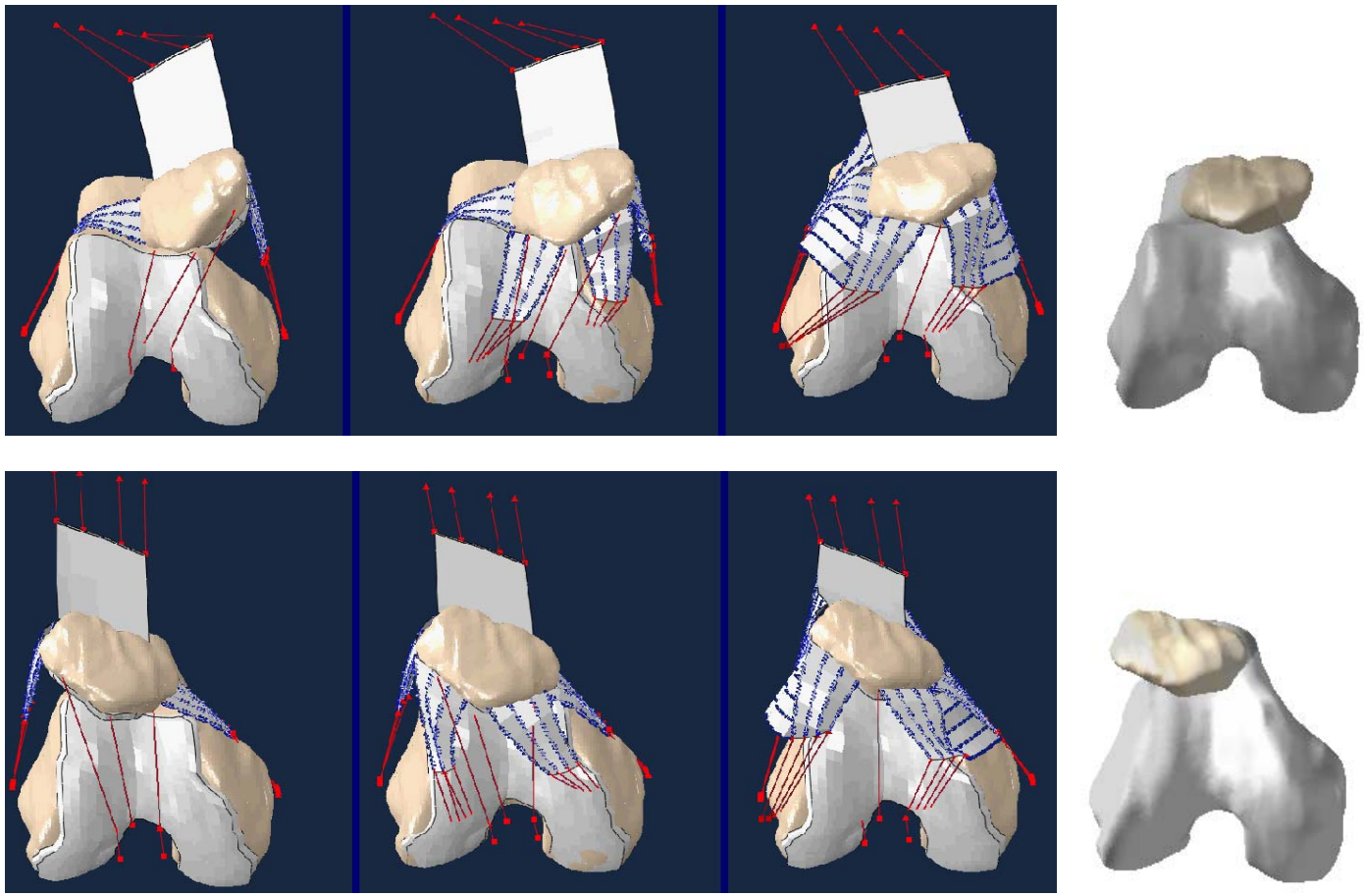

Figure 3.8 Visualization of the final time step for the medial (top) and lateral (bottom) PF laxity models in full extension for iterations #1, #2, & #3, and the corresponding cadaveric experiment.

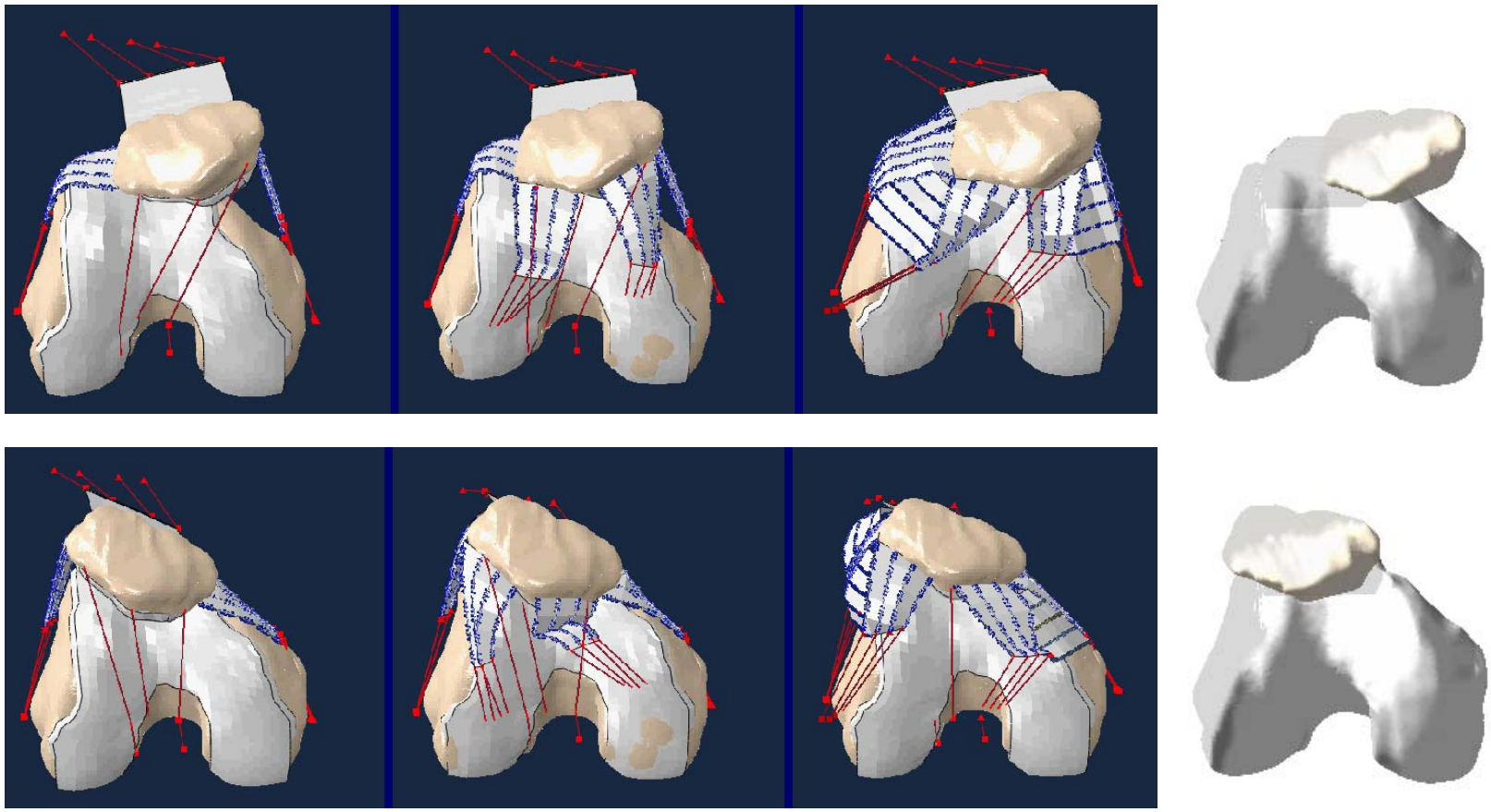

Figure 3.9 Visualization of the final time step for the medial (top) and lateral (bottom) PF laxity models at ~25 degrees for iterations #1, #2, & #3, and the corresponding cadaveric experiment.

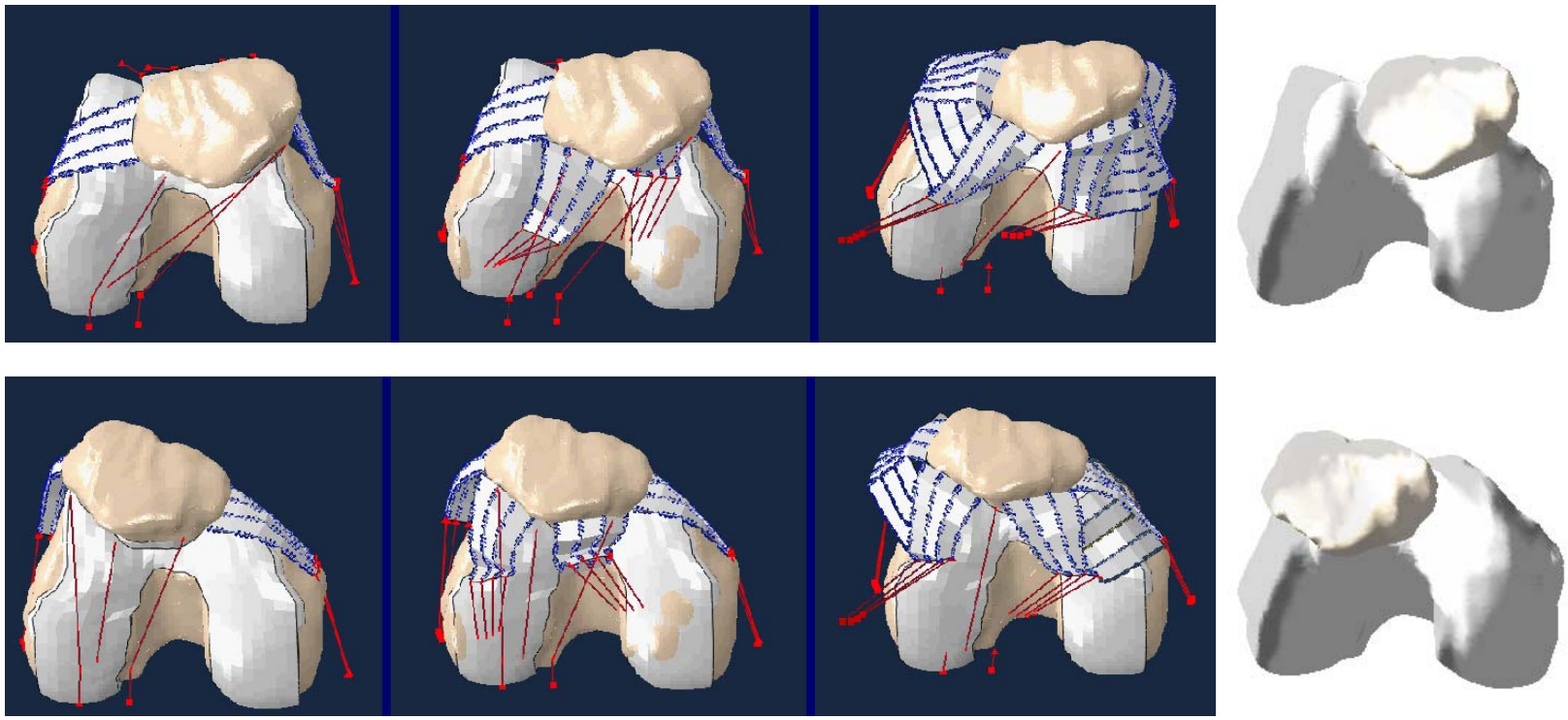

Figure 3.10 Visualization of the final time step for the medial (top) and lateral (bottom) PF laxity models at ~60 degrees for iterations #1, #2, & #3, and the corresponding cadaveric experiment.

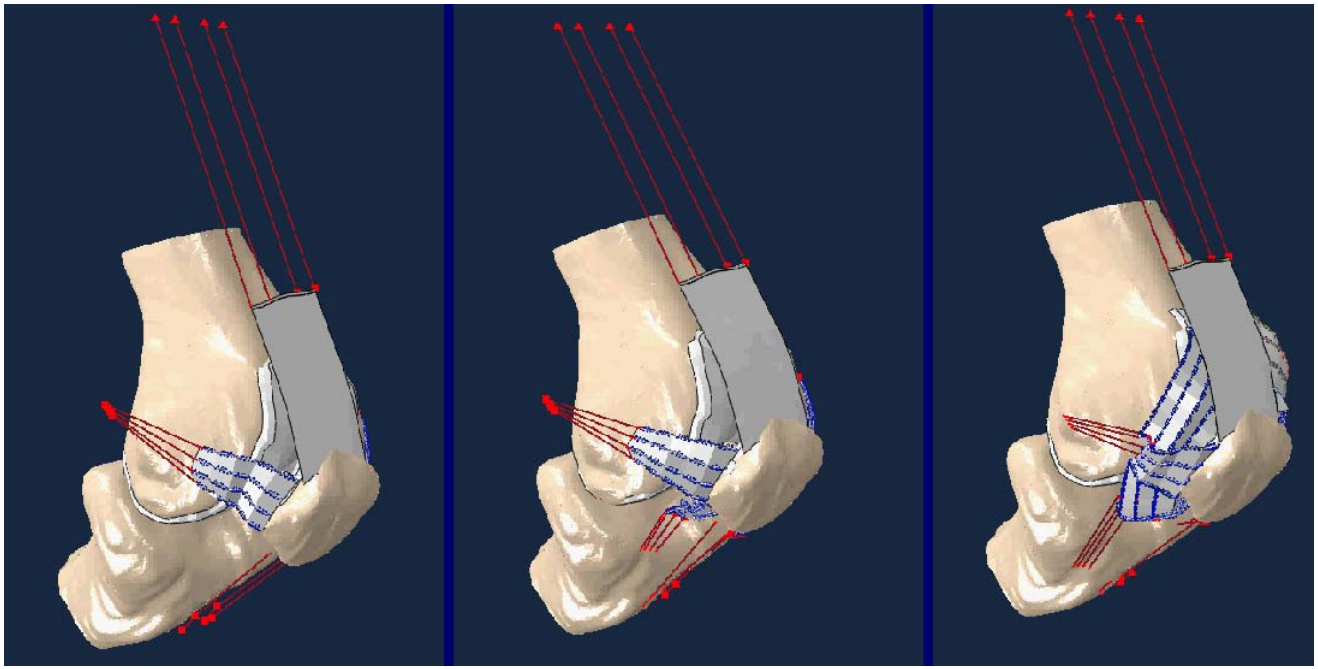

Figure 3.11 Visualization of the final time step for the passive ROM PF laxity models at for iterations #1, #2, & #3.

CHAPTER FOUR: DISCUSSION

A subject specific FE model was developed to predict the patellar kinematics recorded during cadaveric PF laxity experiments. The development of the PF laxity model involved a sequential process in which the soft-tissue was represented with an increasingly more mechanistic approach at each model iteration. The first PF laxity model included soft-tissue representation for the rectus femoris, patella tendon, and patellofemoral ligaments (Figure 2.8). The second and third model iterations added the patellomeniscal ligaments (Figure 2.9) and the retinacular capsule (Figure 2.10), respectively. Optimization was conducted to fine-tune a selection of soft-tissue parameters in order to minimize the difference between model-predicted and experimental kinematic results. The average RMS differences for all flexion angles tested were 2.4 mm and 6.7 degrees with first model iteration, 2.5 mm and 5.4 degrees with the second model iteration, and 2.5 mm and 5.2 degrees with the third model iteration. When the RMS results for medial and lateral PF laxity models are isolated, an improvement is noticed for third iteration's medial laxity results with average RMS differences of 1.6 mm and 4.4 degrees. However, the improvements achieved in terms of translational RMS results for medial PF laxity models were offset with a larger average RMS difference of 3.8 mm for the lateral PF laxity models. The average RMS

differences for patellar rotations sequentially improved for both the medial and lateral PF laxity models.

The differences in average RMS results between the medial and lateral PF laxity models on the third iteration highlight the challenges in correctly fine-tuning the ligaments' parameters for both sides of the knee. When the patella is pushed out of the trochlear groove for a PF laxity test, the geometries of the convex patella bone and convex femoral condyle create an inherently unstable construct, which hence relies on soft-tissue for balance. On one side of the patella the PF ligaments are providing balance by resisting the dislocation force principally in the medial or lateral direction (Figure 4.1). Simultaneously, on the other side of the knee, however, the PF ligaments are applying a force on the patella mainly in the posterior direction and therefore are controlling the IE rotation of the patella. However, when the test is reversed and the patella dislocated in the opposite direction, the PF ligaments on either side of the knee must reverse roles in terms of controlling ML translation and IE rotation. The higher average RMS results the first model iteration demonstrate the limitations in relying primarily on PF ligaments to provide out-of-plane patella constraint. As a potential solution to this challenge, patellomeniscal ligaments and retinacular capsule were added to the soft-tissue representation. The PML's provided additional stability to the patella by applying a reaction force that has a larger component in the SI direction than the PFL's reaction force. The retinacular structure provided stability by tying the rectus femoris, PFL's, and PML's together and through additional soft-tissue wrapping with the distal femur. This soft-tissue representation more closely resembled the interconnected

network of ligaments that forms the natural retinaculum of the knee. For the final iteration of the PF laxity model, optimization was only conducted for the medial PF laxity tests in order to determine the accuracy that could be obtained by focusing on one-sided laxity simulations.

Structures that are not represented in the current PF laxity model but may contribute to PF stability are the patellotibial ligaments, various heads of the quadriceps mechanism (i.e. vastus medialis and vastus lateralis), iliotibial band, multiple layers of the retinaculum, and skin. Also, a more anatomic representation of the patella tendon and extending the retinaculum beyond the anterior portion of the knee may also contribute PF laxity. The patellotibial ligaments were not represented in the current model due to findings by Conlan et al. (1993) and Desio et al. (1998) that demonstrated that the patellotibial ligaments provided only a small percentage of the overall stability. Also, the model did not include the various heads of the quadriceps nor the iliotibial band because these dynamic stabilizers were not loaded in the muscle rig during the cadaveric experiments. Improved anatomic representation of the skin and retinaculum both in terms of layers and a contiguous structure surrounding the knee were considered for the PF laxity models. However, challenges exist in developing these structures to provide adequate wrapping and pre-tension, and in choosing the appropriate parameters for fine-tuning. Nevertheless, due to the nature of extreme out-of-plane patellar motions where the patella is dislocated by 10 mm or more, the retinaculum and skin may provide the stability needed to more accurately predict patellar kinematics. Future work should consider these additional structures.

Further recommendations for future work include modifications to the experimental protocol. As previously mentioned, the entire quadriceps mechanism and IT band play roles in stabilizing the patella (Senavongse and Amis 2005, Merican and Amis 2009); however, they were not loaded in the cadaveric rig. Also, the muscles were resected down to the level of their distal attachments, effectively removing them from the cadaveric knee. These structures should be included in the experiment either by actively applying forces through the rig or by maintaining their proximal attachment points on the hip in order to maintain the integrity of the muscles' excursion capability. As shown in Figure 2.4, the maximum patellar translation was over 15 mm in both medial and lateral translation. This large amount of dislocation might be typical of a knee with a history of patella subluxation, but not to a normal healthy knee. Even so, the patella was able to be displaced with a relatively small force of 44.5 N. The absence of the IT band and quadriceps' complex may be the cause of the increased laxity in the experiment. The IT band especially should be prioritized for addition to the muscle loading rig due the fact that studies have shown that the iliotibial band-patella fibers are significantly stronger than other lateral ligaments (Merican et al. 2009) and the clinical relevance of lateral retinacular tightness leading to lateral release during total knee arthroplasty.

Another recommendation for improvement to the experimental protocol is to create a single point on the patella for application of the custom laxity instrument. This point can easily be created by drilling a small divot in the medial and lateral sides of the patella. A consistent location for applying the load will provide more fidelity between the computational model and experiment.

Review of the literature shows that the majority of knee computational modeling efforts have focused on normal knee activities, such as a deep knee bend or gait, that result in patella kinematics that occur mostly in the sagittal plane (Lanovaz and Ellis 2009, Elias et al. 2004, 2006, and 2010, Mesfar and Shirazi-Adl 2005). Baldwin et al. (2009 & 2012) developed subject specific FE models based on the experimental data from a deep knee bend activity in the Kansas Knee simulator (KKS). The isolated PF model (2009) was able to achieve RMS differences of less than 1.7 mm and 3.1 degrees. The methods used by Baldwin were similar to those employed in the current study. For instance, soft-tissues were represented using a fiber reinforced composite material model, which consists of non-linear springs embedded into a two-dimensional (2D) membrane element. The ligament attachment sites and pre-tension values were parameterized to minimize the difference between the model predicted kinematics and experimental results, and rigid representation was utilized for the articular cartilage. The process in the full KKS model's development also included iterative addition of TF ligaments and optimizing their parameters until the kinematic differences between the experiment and model were sufficiently minimized.

In contrast to the previously mentioned studies, the current work validated peri-patellar soft-tissue representations using data from PF laxity experiments, in which the patella is forced out of the trochlear groove in either the medial or lateral direction. In these experiments, the patella is not able to rely on the relative stability of the concave trochlear groove to determine kinematics as in a deep knee bend. Instead the inherently unstable motion of the patella sliding over the convex femoral condyle produces a

scenario where the soft-tissues provide the majority of PF stability. Hence, the accuracy of the PF laxity model is more dependent on appropriately modeling the supporting soft-tissues.

The PF laxity computational model may provide an efficient method of investigating new designs for medical devices, such as total knee replacements (TKR). Other methods, such as evaluation in cadavers can be costly and time consuming, and present challenges to fully optimizing design features. However, the PF computational model can complete one analysis in approximately six minutes, allowing thousands of analyses to be completed in a reasonable time frame. The PF laxity model may be especially relevant in terms of TKR changes to the trochlear groove geometry. Contemporary TKR designs have been able to reduce the rate of lateral release that was recorded in previous decades (Ballantyne et al. 2003, Kavolus et al. 2008). The reduction in lateral releases was likely a function of both improved implant design and surgical technique. However, as TKR design advances, opportunities may exist in further refining the geometry of the trochlear groove for improved patient performance. A validated PF model provides opportunity to investigate how the TKR's modified trochlear geometry may affect the soft-tissue surrounding the knee and, subsequently, patellar tracking.

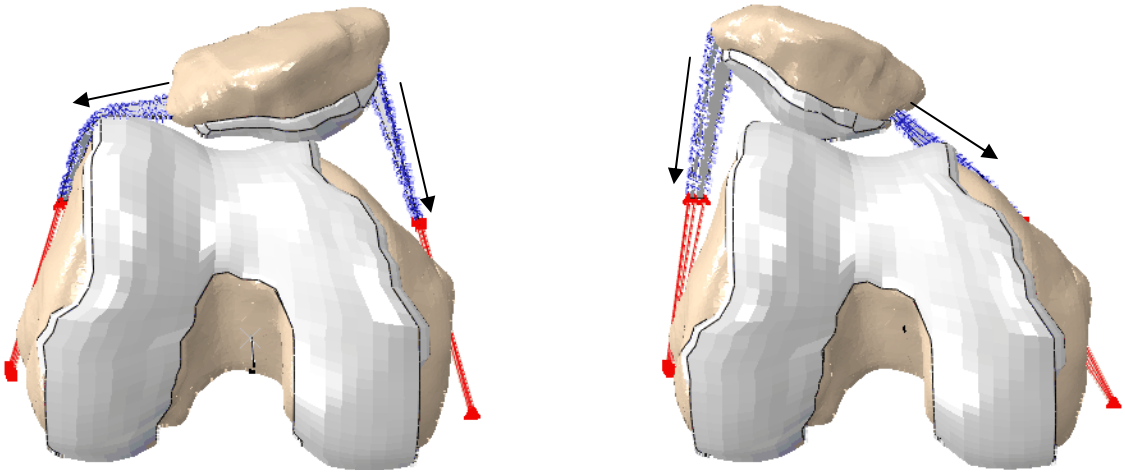

Figure 4.1 Medial and lateral PF laxity models for the ~25 degree flexion angle are shown at full subluxation of the patella. Both PF ligaments must play dual roles in stabilizing the patella in the ML oriented and SI oriented directions depending on whether the patella is subluxed medially or laterally.

CHAPTER FIVE: SUMMARY

Many people suffer from knee pain due to abnormal function of the patellofemoral joint and are not able to enjoy normal activities of daily living. Surgical treatments are available and new methods are being developed by the medical industry. However, computational tools to efficiently evaluate the effects of the intervention on patellofemoral function are lacking.

Historically, computational models of the PF joint have been developed and employed to accomplish various objectives such as investigating joint forces, contact mechanics, and/or kinematics. However, the majority of computational modeling efforts have focused on replicating normal knee activities, such as a deep knee bend or gait, that result in patella kinematics that occur mostly in the sagittal plane. To date, no developments have been reported in the literature that focus on validating computational models of passive patellofemoral constraint. Therefore, the present study to developed a computationally efficient model of the patellofemoral joint that was validated with out-of-plane motion of the patella recorded during cadaver PF laxity simulations.

A subject specific FE model was developed to predict the patellar kinematics recorded during cadaveric PF laxity experiments. Medial and lateral PF laxity models were developed with the knee positioned in full extension and flexed to approximately 25 and 60 degrees. A model to simulate passive range of motion was also created. The development of the PF laxity model involved a sequential process in which the soft-tissue

was represented with an increasingly more mechanistic approach at each model iteration. Optimization was conducted to fine-tune a selection of soft-tissue parameters in order to minimize the difference between model-predicted and experimental kinematic results. The average RMS differences for all flexion angles tested were 2.4 mm and 6.7 degrees with first model iteration, 2.5 mm and 5.4 degrees with the second model iteration, and 2.5 mm and 5.2 degrees with the third model iteration. When the RMS results for medial and lateral PF laxity models are isolated, an improvement is noticed for third iteration's medial laxity results with average RMS differences of 1.6 mm and 4.4 degrees. However, the improvements achieved in terms of translational RMS results for medial PF laxity models were offset with a larger average RMS difference of 3.8 mm for the lateral PF laxity models. The average RMS differences for patellar rotations sequentially improved for both the medial and lateral PF laxity models.

The PF laxity computational model may provide an efficient method of investigating new designs for medical devices, such as total knee replacements (TKR). The PF laxity model may be especially relevant in terms of TKR changes to the trochlear groove geometry. Contemporary TKR designs have been able to reduce the rate of lateral release that was recorded in previous decades (Ballantyne et al. 2003, Kavolus et al. 2008). The reduction in lateral releases was likely a function of both improved implant design and surgical technique. However, as TKR design advances, opportunities may exist to further refine the geometry of the trochlear groove for improved patient performance. A validated PF model provides the opportunity to investigate how the

TKR's modified trochlear geometry may affect the soft-tissue surrounding the knee and, subsequently, patellar tracking.

REFERENCES

Amis, A. A., P. Firer, J. Mountney, W. Senavongse, and N. P. Thomas. 2003. "Anatomy and Biomechanics of the Medial Patellofemoral Ligament." *Knee* 10 (3): 215-220.

Amis, A. A., W. Senavongse, and A. M. J. Bull. 2006. "Patellofemoral Kinematics during Knee Flexion-Extension: An in Vitro Study." J*ournal of Orthopaedic Research* 24 (12): 2201-2211.

Atkinson, P., Atkinson, T., Huang, C., Doane, R., 2000. A comparison of the mechanical and dimensional properties of the human medial and lateral patellofemoral ligaments. 46th Annual Meeting of the Orthopaedic Research Society 0776.

Baldwin, J. L. 2009. "The Anatomy of the Medial Patellofemoral Ligament." *American Journal of Sports Medicine* 37 (12): 2355-2361.

Baldwin, M. A., C. Clary, L. P. Maletsky, and P. J. Rullkoetter. 2009a. "Verification of Predicted Specimen-Specific Natural and Implanted Patellofemoral Kinematics during Simulated Deep Knee Bend." *Journal of Biomechanics* 42 (14): 2341-2348.

Baldwin, M. A., P. J. Laz, J. Q. Stowe, and P. J. Rullkoetter. 2009b. "Efficient Probabilistic Representation of Tibiofemoral Soft Tissue Constraint." *Computer Methods in Biomechanics and Biomedical Engineering* 12 (6): 651-659.

Ballantyne, A., J. McKinley, and I. Brenkel. 2003. "Comparison of the Lateral Release Rates in the Press Fit Condylar Prosthesis and the PFC Sigma Prosthesis." *Knee* 10 (2): 193-198.

Barink, M., S. Van de Groes, N. Verdonschot, and M. De Waal Malefijt. 2003. "The Trochlea is Bilinear and Oriented Medially." *Clinical Orthopaedics and Related Research* (411): 288-295.

Blankevoort, L., J. H. Kuiper, R. Huiskes, and H. J. Grootenboer. 1991. "Articular Contact in a Three-Dimensional Model of the Knee." *Journal of Biomechanics* 24 (11): 1019-1031.

Caruntu, D. I. and M. S. Hefzy. 2004. "3-D Anatomically Based Dynamic Modeling of the Human Knee to Include Tibio-Femoral and Patello-Femoral Joints." *Journal of Biomechanical Engineering* 126 (1): 44-53.

Clary, C.W., 2009. “A Combined Experimental-Computational Method to Generate Reliable Subject Specific Models of the Knee’s Ligamentous Constraint.” Ph.D. diss., University of Kansas.

Conlan, T., W. P. Garth Jr., and J. E. Lemons. 1993. "Evaluation of the Medial Soft-Tissue Restraints of the Extensor Mechanism of the Knee." *Journal of Bone and Joint Surgery - Series A* 75 (5): 682-693.

Desio, S. M., R. T. Burks, and K. N. Bachus. 1998. "Soft Tissue Restraints to Lateral Patellar Translation in the Human Knee." *American Journal of Sports Medicine* 26 (1): 59-65.

Dhaher, Y. Y. and L. E. Kahn. 2002. "The Effect of Vastus Medialis Forces on Patello-Femoral Contact: A Model-Based Study." *Journal of Biomechanical Engineering* 124 (6): 758-767.

Dirim, B., P. Haghighi, D. Trudell, G. Portes, and D. Resnick. 2008. "Medial Patellofemoral Ligament: Cadaveric Investigation of Anatomy with MRI, MR Arthrography, and Histologic Correlation." *American Journal of Roentgenology* 191 (2): 490-498.

Elias, J. J., D. R. Bratton, D. M. Weinstein, and A. J. Cosgarea. 2006. "Comparing Two Estimations of the Quadriceps Force Distribution for use during Patellofemoral Simulation." *Journal of Biomechanics* 39 (5): 865-872.

Elias, J. J., S. Kilambi, and A. J. Cosgarea. 2010. "Computational Assessment of the Influence of Vastus Medialis Obliquus Function on Patellofemoral Pressures: Model Evaluation." *Journal of Biomechanics* 43 (4): 612-617.

Elias, J. J., D. R. Wilson, R. Adamson, and A. J. Cosgarea. 2004. "Evaluation of a Computational Model used to Predict the Patellofemoral Contact Pressure Distribution." *Journal of Biomechanics* 37 (3): 295-302.

Farahmand, F., W. Senavongse, and A. A. Amis. 1998. "Quantitative Study of the Quadriceps Muscles and Trochlear Groove Geometry Related to Instability of the Patellofemoral Joint." *Journal of Orthopaedic Research* 16 (1): 136-143.

Fithian, D. C., E. Nomura, and E. Arendt. 2001. "Anatomy of Patellar Dislocation." *Operative Techniques in Sports Medicine* 9 (3): 102-111.

Gray, H. 1918 Gray's Anatomy of the Human Body 20th edition. Lea & Febiger, Philidelphia, PA. (Retrieved from http://commons.wikimedia.org; Images have lapsed into the public domain)

Grood, E.S., and W. J. Suntay, 1983. "Joint coordinate system for the clinical description of three-dimensional motions: application to the knee." J*ournal of Biomechanical Engineering* 105, 136–144.

Iranpour, F., A. M. Merican, W. Dandachli, A. A. Amis, and J. P. Cobb. 2010. "The Geometry of the Trochlear Groove." *Clinical Orthopaedics and Related Research* 468 (3): 782-788.

Komosa, M.C., S.S. Shalhoub, A.J. Cyr, and L.P. Maletsky. 2011. "Assessment of in Vitro Patellar Laxity in the Native Knee." *Proceedings of the ASME 2011 Summer Bioengineering Conference*, Farmington, PA, June 22-25.

Kavolus, C. H., M. T. Hummel, K. P. Barnett, and J. E. Jennings Jr. 2008. "Comparison of the Insall-Burstein II and NexGen Legacy Total Knee Arthroplasty Systems with Respect to Patella Complications." *Journal of Arthroplasty* 23 (6): 822-825.

Lanovaz, J. L. and R. E. Ellis. 2009. "A Cadaverically Evaluated Dynamic FEM Model of Closed-Chain TKR Mechanics." *Journal of Biomechanical Engineering* 131 (5).

LaPrade, R. F., A. H. Engebretsen, T. V. Ly, S. Johansen, F. A. Wentorf, and L. Engebretsen. 2007. "The Anatomy of the Medial Part of the Knee." *Journal of Bone and Joint Surgery - Series A* 89 (9): 2000-2010.

Maletsky, L. P. and B. M. Hillberry. 2005. "Simulating Dynamic Activities using a Five-Axis Knee Simulator." *Journal of Biomechanical Engineering* 127 (1): 123-133.

Merican, A. M. and A. A. Amis. 2008. "Anatomy of the Lateral Retinaculum of the Knee." *Journal of Bone and Joint Surgery - Series B* 90 (4): 527-534.

Merican, A. M. and A. A. Amis. 2009. "Iliotibial Band Tension Affects Patellofemoral and Tibiofemoral Kinematics." *Journal of Biomechanics* 42 (10): 1539-1546.

Merican, A. M., S. Sanghavi, F. Iranpour, and A. A. Amis. 2009. "The Structural Properties of the Lateral Retinaculum and Capsular Complex of the Knee." *Journal of Biomechanics* 42 (14): 2323-2329.

Mesfar, W. and A. Shirazi-Adl. 2005. "Biomechanics of the Knee Joint in Flexion Under various Quadriceps Forces." *Knee* 12 (6): 424-434.

Mountney, J., W. Senavongse, A. A. Amis, and N. P. Thomas. 2005. "Tensile Strength of the Medial Patellofemoral Ligament before and After Repair Or Reconstruction." *Journal of Bone and Joint Surgery - Series B* 87 (1): 36-40.

Nomura, E., Y. Horiuchi, and M. Kihara. 2000. "Medial Patellofemoral Ligament Restraint in Lateral Patellar Translation and Reconstruction." *Knee* 7 (2): 121-127.

Nomura, E., M. Inoue, and N. Osada. 2005. "Anatomical Analysis of the Medial Patellofemoral Ligament of the Knee, especially the Femoral Attachment." *Knee Surgery, Sports Traumatology, Arthroscopy* 13 (7): 510-515.

Philippot, R., B. Boyer, R. Testa, F. Farizon, and B. Moyen. 2012. "The Role of the Medial Ligamentous Structures on Patellar Tracking during Knee Flexion." *Knee Surgery, Sports Traumatology, Arthroscopy* 20 (2): 331-336.

Philippot, R., J. Chouteau, J. Wegrzyn, R. Testa, M. H. Fessy, and B. Moyen. 2009. "Medial Patellofemoral Ligament Anatomy: Implications for its Surgical Reconstruction." *Knee Surgery, Sports Traumatology, Arthroscopy* 17 (5): 475-479.

Powers, C. M., Y. -J Chen, I. Scher, and T. Q. Lee. 2006. "The Influence of Patellofemoral Joint Contact Geometry on the Modeling of Three Dimensional Patellofemoral Joint Forces." *Journal of Biomechanics* 39 (15): 2783-2791.

Senavongse, W. and A. A. Amis. 2005. "The Effects of Articular, Retinacular, Or Muscular Deficiencies on Patellofemoral Joint Stabilitiy." *Journal of Bone and Joint Surgery - Series B* 87 (4): 577-582.

Shih, Y. -F, A. M. J. Bull, and A. A. Amis. 2004. "The Cartilaginous and Osseous Geometry of the Femoral Trochlear Groove." *Knee Surgery, Sports Traumatology, Arthroscopy* 12 (4): 300-306.

Stäubli, H. U., L. Schatzmann, P. Brunner, L. Rincón, and L. -P Nolte. 1999. "Mechanical Tensile Properties of the Quadriceps Tendon and Patellar Ligament in Young Adults." *American Journal of Sports Medicine* 27 (1): 27-34.

Stephen, J. M., P. Lumpaopong, D. J. Deehan, D. Kader, and A. A. Amis. 2012. "The Medial Patellofemoral Ligament: Location of Femoral Attachment and Length Change Patterns Resulting from Anatomic and Nonanatomic Attachments." *American Journal of Sports Medicine* 40 (8): 1871-1879.

Tecklenburg, K., D. Dejour, C. Hoser, and C. Fink. 2006. "Bony and Cartilaginous Anatomy of the Patellofemoral Joint." *Knee Surgery, Sports Traumatology, Arthroscopy* 14 (3): 235-240.

Terry, G. C. 1989. "The Anatomy of the Extensor Mechanism." *Clinics in Sports Medicine* 8 (2): 163-177.

Thawait, S. K., T. Soldatos, G. K. Thawait, A. J. Cosgarea, J. A. Carrino, and A. Chhabra. 2012. "High Resolution Magnetic Resonance Imaging of the Patellar Retinaculum: Normal Anatomy, Common Injury Patterns, and Pathologies." *Skeletal Radiology* 41 (2): 137-148.

Tuxøe, J. I., M. Teir, S. Winge, and P. L. Nielsen. 2002. "The Medial Patellofemoral Ligament: A Dissection Study." *Knee Surgery, Sports Traumatology, Arthroscopy* 10 (3): 138-140.

Warren, L. F. and J. L. Marshall. 1979. "The Supporting Structures and Layers on the Medial Side of the Knee. an Anatomical Analysis." *Journal of Bone and Joint Surgery - Series A* 61 (1): 56-62.

Yamada, Y., Y. Toritsuka, H. Yoshikawa, K. Sugamoto, S. Horibe, and K. Shino. 2007. "Morphological Analysis of the Femoral Trochlea in Patients with Recurrent Dislocation of the Patella using Three-Dimensional Computer Models." *Journal of Bone and Joint Surgery - Series B* 89 (6): 746-751.

Yoo, J. H., S. R. Yi, and J. H. Kim. 2007. "The Geometry of Patella and Patellar Tendon Measured on Knee MRI." *Surgical and Radiologic Anatomy* 29 (8): 623-628.